Master's thesis

NTNU
Norwegian University of Science and Technology
Faculty of Natural Sciences
Department of Biotechnology and Food Science

Tove Enmo Bugge

Use of atomic force microscopy to study bacterial adhesion to mucins

Master's thesis in Biotechnology

Supervisor: Marit Sletmoen

August 2020

NTNU
Norwegian University of Science and Technology

Tove Enmo Bugge

Use of atomic force microscopy to study bacterial adhesion to mucins

Master's thesis in Biotechnology
Supervisor: Marit Sletmoen
August 2020

Norwegian University of Science and Technology
Faculty of Natural Sciences
Department of Biotechnology and Food Science

NTNU
Norwegian University of
Science and Technology

Acknowledgments

This is the final thesis of the Master of Science program in Biotechnology at the Norwegian University of Science and Technology (NTNU), at the department of Biotechnology and Food Science. The research was conducted between August 2019 to August 2020.

I would like to thank my supervisor, Marit Sletmoen, for excellent guidance and feedback during this project. I would also like to thank Karen Dunker for the guidance and support in the laboratory, and for all the things she taught me about the AFM and the experimental methods. Both of you have supported me with kind words and reassurement during the whole process. I would also like to thank the members of the Micromucus project for great insight and info.

I would also like to thank my family and boyfriend, Jonas, for all support, and classmates Ann Isabel, Renate and Hanne, for all the great moments during my two years at NTNU.

Tove Enmo Bugge Trondheim, August 2020

Abstract

The mucosal barrier, covering the respiratory, gastrointestinal, and urogenital systems in higher organisms, plays an important part in the first line of defence against environmental dangers. Mucus also cover the skin of amphibians, snails, and fish. A major component in mucus is the glycoprotein mucin, which is responsible for the viscoelastic properties of the mucus. The mucin molecules are a major target for both microbiota and parasites and serve as a carbon and energy source for the bacteria. Bacteria have developed a high number of mechanisms to colonize their target surface, and it is important to study the adhesive properties of bacteria to better understand how they affect their host.

The aim of this thesis was to investigate the bacterial adhesion of *Arthrobacter* and *Janthinobacterium* to mucins isolated from mucosal surfaces found in pig (PGM) and bovine (BSM). Bacterial adhesion was measured with atomic force microscopy (AFM). AFM is a well-suited tool for studying bacteria adhesion to mucins as it allows measurements with live cells and measurements of single molecular interactions in the nanometer scale. This master thesis includes a comparison of the adhesion properties before and after the mucins are treated with neuraminidase, an enzyme that removes sialic acid units from glycan chains. We hypothesized that the bacteria would interact with the glycans on the mucins. We expected the neuraminidase treatment to alter the mucin-properties, thus also affecting bacterial adhesion. Single molecular pair interactions were also analysed to identify the rupture force of single interaction.

Force curves were obtained with AFM, and deadhesion work and rupture forces of the bacterial interaction with the mucins was determined. The results indicated that the binding strength of both *Arthrobacter* and *Janthinobacterium* to both mucins was weak. For both bacteria, the binding strength was slightly stronger to BSM than PGM. The adhesive properties of *Arthrobacter* were reduced after neuraminidase treatment of the mucins, but the adhesive properties of *Janthinobacterium* were elevated. When measuring single molecular pair interactions, the rupture force of the molecular bonds formed between both bacteria and the mucin coated surfaces were in the interval of 0,1 – 0,3 or 0,4 nN. These results are in line with previous studies.

Sammendrag

I høyere organismers indre organer, som luftveiene, mage- og tarmkanalen og det urogenitale system, dekkes overflateepitel av et slimlag, også kalt mucus. Mucus dekker også huden til amfibier, snegler og fisk. Mucus spiller en viktig rolle som en beskyttende barriere mot omgivelsene. En hovedkomponent i mucus er glykoproteinet mucin, som gir opphav til de viskoelastiske egenskapene til mucus. Muciner er et viktig mål for både normalflora og parasitter, og tjener som en kilde til karbon og energi for bakterier. Bakterier har utviklet en rekke mekanismer for å sikre kolonisering på måloverflater, og å studere egenskapene bak bakterieadhesjon er viktig for å forstå hvordan bakterier påvirker verten.

Målet med denne oppgaven var å undersøke *Arthrobacters* og *Janthinobacteriums* adhesjon til muciner isolert fra mucusdekte overflater hos storfe (BSM) og gris (PGM). Bakterieadhesjon ble målt ved bruk av atomkraftmikroskopi (AFM). AFM er et velegnet verktøy for å studere bakterieadhesjon til muciner. Metoden tillater målinger med levende celler, og målinger av enkeltmolekylære interaksjoner i nanometerskalaen. I denne oppgaven sammenlignes adhesjonsegenskaper til bakteriene før og etter mucinene ble behandlet med neuramindase, et enzym som fjerner sialinsyreenheter fra glykankjeder. Vi antok at bakteriene ville interagere med glykaner på mucinene, og at neuraminidasebehandlingen ville endre egenskapene til mucinene og påvirke bakterieadhesjon. Enkeltmolekylære par-interaksjoner ble analysert for å identifisere bruddkraften til enkle interaksjoner.

Kraftkurver fra AFM-målinger ble brukt for å bestemme deadhesionsarbeid og bruddkraften for bakterieinteraksjonen med mucinene. Resultatet indikerte at bindingsstyrken for både *Arthrobacter* og *Janthinobacterium* var svake til begge mucinene, men den var noe sterkere til BSM enn PGM. Etter behandling av mucinene med neuraminidase ble *Arthrobacters* adhesjonsegenskaper redusert, mens *Janthinobacteriums* adhesjonsegenskaper økte. Ved måling av enkeltmolekylære par-interaksjoner, ble bruddkraften til de molekylære bindingene mellom bakteriene og mucinene målt til å ligge i intervallet 0,1 – 0,3 eller 0,4 nN. Disse resultatene samsvarer med tidligere studier.

Table of contents

Acknowledgments i
Abstract iii
Sammendrag v
Table of contents vii
Abbreviation ix
1. Introduction 1
1.1 Background 1
1.2 Mucus 1
1.2.1 Mucins 2
1.2.2 Bovine submaxillary mucin (BSM) and porcine gastric mucin (PGM) 3
1.3 Neuraminidase 4
1.4 Bacterial adhesion 4
1.4.1 Bacterial adhesion to target surfaces and mucins 5
1.4.2 Biofilms 6
1.4.3 *Arthrobacter* and *Janthinobacterium* 6
2. Experimental methods 7
2.1 Atomic force microscopy (AFM) 7
2.1.1 AFM components 7
2.1.2 Force spectroscopy 9
2.2 Fluorescence microscopy 10
2.2.1 Components of the fluorescence microscope 11
2.3 Immobilisation of bacteria and mucins 11
2.3.1 Polydopamine 11
2.3.2 Silanes 12
3. Materials and methods 13
3.1 List of chemicals 13
3.2 Bacterial immobilisation to AFM cantilever 14
3.2.1 Cultivation of bacteria 14
3.2.2 Immobilisation of *Janthinobacterium* and *Arthrobacter* to AFM cantilever 14
3.2.2 Live/dead assay of immobilized bacteria 14
3.3 Preparation of mucin-coated mica sheets 15
3.3.1 Immobilisation of BSM and PGM mucins on mica sheets 15
3.3.2 Neuraminidase treatment of BSM and PGM 15
3.4 AFM measurements of bacterial adhesion to mucins 15

3.4.1 Analysis of AFM force curves 16
4. Results 17
4.1 Bacterial immobilisation to AFM cantilever 17
4.1.1 Cultivation of bacteria 17
4.1.2 Immobilisation of *Janthinobacterium* and *Arthrobacter* to AFM cantilever 17
4.1.3 Live/dead assay of immobilized bacteria 17
4.2 AFM measurements of bacterial adhesion to mucins 20
4.2.1 Bacterial adhesion to BSM and PGM 20
4.3.2 Comparison of bacterial adhesion and force curves 22
4.3.3 Analysis of single molecular pair interactions 24
5. Discussion 29
5.1 Bacterial immobilisation to AFM cantilever 29
5.2 Bacterial adhesion to BSM and PGM 30
5.2.1 Bacterial adhesion to BSM and PGM treated with neuraminidase 31
5.3 Single molecular pair interactions 33
6. Conclusion 35
Bibliography 37
Appendix 41
Solutions and media 41

Abbreviations

AFM	Atomic force microscopy
BSM	Bovine submaxillary mucin
EDC	N-(3-dimethylaminopropyl)-N’-ethylcarbodiimide hydrochloride
Gal	Galactose
GalNAc	N-Acetylgalactosamine
GlcNAc	N-Acetylglucosamine
PDA	Polydopamine
PGM	Porcine gastric mucine
SGM	Salmon gnotobiotic medium
TSA	Tryptic soy agar
TSB	Tryptic soy broth

1. Introduction

1.1 Background

The mucosal barrier of fish and higher organisms plays a crucial part in the first line of defence, and functions as a protective barrier that shields the host against environmental dangers (Barr *et al.*, 2015). The microbiota often interacts with the mucosal barrier, and the host-microbiota commensalism plays a major part in health and protection against foreign pathogens (Sicard *et al.*, 2017). Investigating these interaction properties is thus of great importance for understanding how bacteria affects other living organisms.

The human intestinal tract is covered with mucus, which functions as a protective layer that hinders bacteria from invading the epithelium. The intestinal tract is also covered in microbiota, which has multiple beneficial properties for the host such as defence and digestion (Van den Abbeele *et al.*, 2012). The microbiota can use the mucus as an energy source, and they can affect the mucosal composition and release to benefit the microbe and the host (Sicard *et al.*, 2017). Bacteria's ability to adhere to mucins plays an important role in colonization, and bacterial binding properties affects the body's commensal bacteria flora.

Bacterial colonization of the host depends on the bacteria's ability to interact with and adhere to the target surface, and both commensal and pathogenic microbes have developed a great number of adhesive mechanism. Many bacteria adhere to host glycans, and multiple bacteria recognize and binds to the glycoprotein mucin in the mucosal layer (Berg *et al.*, 2002). It is therefore of great interest to investigate the mechanism behind these adhesion properties.

Atomic force microscopy (AFM) is a great tool for studying bacterial adhesion to mucins. AFM allows measurements with live cells, and to measure single molecular interactions in the nanometer scale (Chang *et al.*, 2012). The aim of this thesis is to investigate bacterial adhesion to mucins isolated from mucosal surfaces found in pig and bovine with AFM. The study also includes a comparison of the adhesion properties before and after the mucins are treated with neuraminidase, an enzyme that removes sialic acid units from the glycan chains of mucins.

1.2 Mucus

Mucus is an aqueous secretion commonly found in the columnar epithelia of the respiratory, gastrointestinal, and urogenital system in higher organisms (Ambort *et al.*, 2012). The mucus functions as a defensive barrier between the host and the external environment and is an important part of the primary host defence system (Barr *et al.*, 2015). The mucus also helps maintaining the hydrated layer over the epithelium, and it serves as a lubricant which helps with matter passage (Bansil and Turner, 2006). Epidermal mucus is also found to covers the skin of some organisms, such as amphibians, snails, and fish. Fish and other sea creatures live in direct contact with their environment, and an outer mucus layer benefits them as it helps prevent infection by parasites and other microbes (Esteban, 2012)**.**

In the columnar epithelia, mucus is synthesised by goblet cells or mucous cells. The mucus is stored within granules and are secreted upon external signals (Bansil and Turner, 2018). The mucus is continuously released and renewed, which helps prevent congestion of excess microbes and thus infection (Esteban, 2012). It is of great importance for the host that the mucosal layer function properly and is undistorted. If the mucus is impaired or damaged the protective properties will decrease, and pathogens may breach the mucosal barrier and cause disease (Barr *et al.*, 2015).

The mucus is made up of ~ 95% water, but many of the essential properties of the mucus such as its viscosity and gel-like properties are due to the glycoprotein mucin (Bansil and Turner, 2006). The properties of mucins allows them to function as an interacting medium with the microflora and other microbes (Corfield, 2015). Other components commonly found in mucus are salts and lipids, and antimicrobial molecules like immunoglobulins, lysozymes and defensins (Bansil and Turner, 2006).

1.2.1 Mucins

Mucins are large O-glycosylated glycoproteins, and their molecular weight ranges from 0.5 to 20 MDa (Bansil and Turner, 2006). They possess strong adhesive properties and play an important part in the mucosal defence system (Esteban, 2012). The protein is characterised by a high level of O-glycosylation at the serine, threonine, and proline residues in the protein backbone (Ambort *et al.*, 2012).

About 80% of the mucin protein mass consists of carbohydrates, which are attached to the protein backbone (Figure 1.1). Each oligosaccharide chain usually contains 5-15 monomers, which commonly is N-acetylgalactosamine (GalNAc), N-acetylglucosamine (GlcNAc), N-acetylneuraminic acid (sialic acid), fucose and galactose (Gal) (Bansil and Turner, 2006). Some have antigenic properties, or function as recognition sites for lectins (Brockhausen and Stanley, 2017). Sialic acids are negatively charged monomers, and they are common terminal residues in carbohydrate chains. They are linked to glycans by α-glycosidic bonds and are often involved in microbial adhesion (Baos *et al.*, 2012). Their negative charge affects cell surface properties and molecular interactions.

O-linked glycosylation of mucins are initiated with the monomer GalNAc, and the simplest chains is composed of only this single GalNAc monomer. These are also known as Tn antigens (Brockhausen and Stanley, 2017). Further elongation varies between the numerous carbohydrate chains, rendering the glycans heterogenous, and the chains can also form a linear or branched arrangement. Most carbohydrate chains are however terminated by sialic acid, fructose, Gal or GalNAc monomers (Lindén *et al.*, 2008).

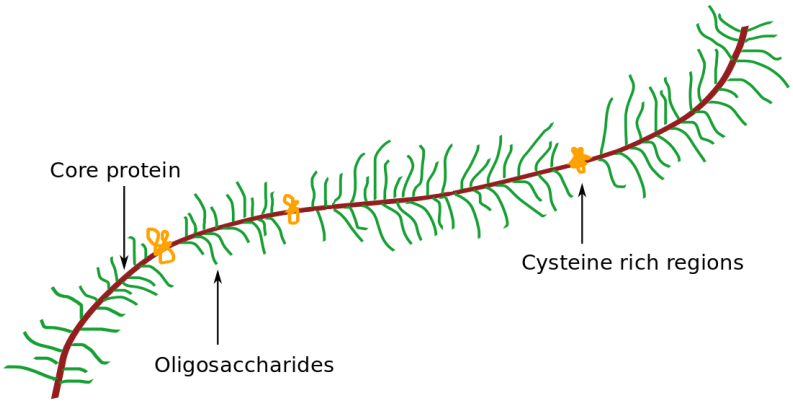

Figure 1.1: Simplified model of an O-glycosylated mucin, containing a protein core, oligosaccharides, and cysteine rich regions. Figure modified from (Erdal, 2019).

The protein backbone of mucins constitutes the remaining 20% of the total protein mass. It consists om a glycosylated central part, and N- and C-terminal unglycosylated regions (Bansil and Turner, 2006). The central region of the protein backbone is rich in PST-domains, contains tandem repeats rich in proline, serine, and threonine, the sites of O-glycosylation (Ambort *et al.*, 2012). Cysteine rich domains are interspersed within the central region as well (Figure 1.1). The terminal regions of mucins are also rich in cysteine, and they both facilitate the formation of disulfide bridges which allows dimerization and polymerisation of mucin molecules. This feature is the foundation of the viscoelastic properties of mucus (Bansil and Turner, 2006). These types of mucins are also referred to as gel-forming mucins, and these are synthesised by goblet cells that line the columnar epithelium (Lindén *et al.*, 2008).

Mucins are divided into cell-surface or membrane-bound mucins, and secreted mucins which are divided as either gel-forming or non-gel-forming (Lindén *et al.*, 2008). All mucins share many of the same traits, though membrane bound mucins additionally contains a hydrophobic transmembrane region, and a cytoplasmic region (Brockhausen and Stanley, 2017). Both groups play an important part in host defence as they make up a protective barrier between the epithelial surface and the external environment. Membrane-bound mucins are expressed in mucosal tissues and are part of the cells glycocalyx, the network of external carbohydrates attached to the cell membrane. (Lindén *et al.*, 2008). Membrane-bound mucins also play an important role in cell signalling (Madsen *et al.*, 2016).

1.2.2 Bovine submaxillary mucin (BSM) and porcine gastric mucin (PGM)

Bovine submaxillary mucin (BSM)

Mucus from bovine submaxillary glands, Type I-S, is isolated from the salivary glands of bovine. The BSM protein backbone is rich in serine, threonine, and proline (Sigma-Aldrich, 2020a). Prevalent glycans are N,O-diacetylneuraminic acid, 2-Acetamido-2-deoxy-D-galactose, and 2-Acetamido-2-deoxy-D-glucose, Fructose and D-galactose are present but not to the same extent. Bound sialic acid is measured to make up 9-24 %, and free sialic acid ≤2.5 %, of the total mass of BSM (Sigma-Aldrich, 2020a). ~30% of the total carbohydrate mass of BSM is composed of sialic acid, which gives the molecule a high concentration of negatively charged carbohydrates (Madsen *et al.*, 2016).

Porcine gastric mucin (PGM)

Mucin from porcine stomach Type III is isolated from pig stomach. ~43% of the amino acids that compose the protein backbone of PGM is serine, threonine and proline, and the glycosylation of carbohydrates occurs especially at the hydroxyl groups of serine and threonine residues (Sigma-Aldrich, 2020b). The protein backbone is estimated to make up 16-20% of the whole PGM molecule, whereas the carbohydrates section makes up 80-84%. Prevalent glycans in PGM are N-acetylgalactosamine, N-acetylglucosamine, Fucose, Galactose, and N-acetylneuraminic acid (Sigma-Aldrich, 2020b). The content of bound sialic acid is estimated to make up 0.5 – 1.5 % of the total PGM mass, which gives PGM a lower density of negatively charged carbohydrates than BSM (Madsen *et al.*, 2016).

1.3 Neuraminidase

Neuraminidase, also known as sialidase, is a group of enzymes that cleaves terminal sialic acids on glycan chains (Glanz *et al.*, 2018). By cleaving sialic acids from glycans, the properties and molecular behaviour of the glycans will be altered. Terminal sialic acids are usually linked to glycans by α-glycosidic bonds by the C2 carbon (Stencel-Baerenwald *et al.*, 2014). Figure 1.2 represents the two most common sialic acids in mammals, *N*-acetylneuraminic acid (Neu5Ac) and hydroxylated Neu5Gc (Glanz *et al.*, 2018).

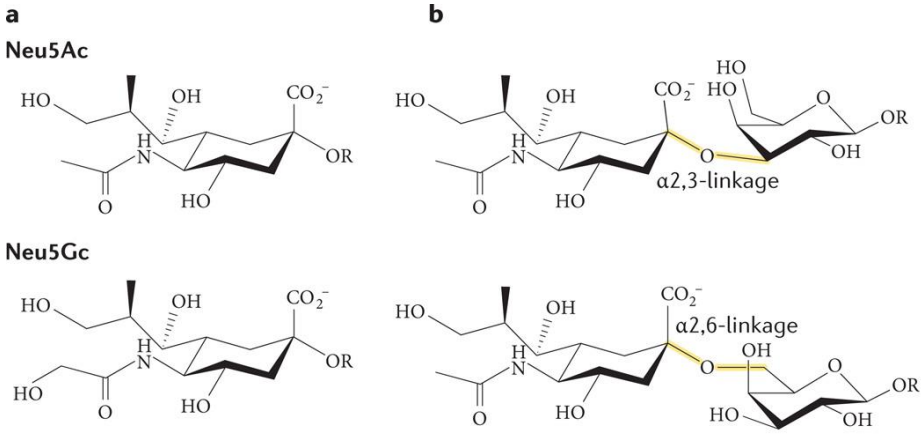

Figure 1.2: Chemical structure of sialic acids and α-glycosidic bonds. a) Illustration of the two most common mammalian sialic acids, *N*-acetyl neuraminic acid (Neu5Ac) and *N*-glycolylneuraminic acid (Neu5Gc). b) Neu5Ac α-glycosidic linked by α-(2,3) and α-(2,6) glycosidic bonds to carbohydrate monomer. Figure modified from (Stencel-Baerenwald *et al.*, 2014).

There are several types of α-glycosidic bonds and various neuraminidases which recognize them, and some enzymes can also recognize multiple different bonds. Mammals produce neuraminidase to be used in various cellular processes, but many microbes and pathogens that depend on interactions with host glycans also produce neuraminidases to facilitate host interaction (Glanz *et al.*, 2018).

α(2→3,6,8,9) Neuraminidase from *Arthrobacter ureafaciens*

The α(2→3,6,8,9) neuraminidase isolated from *Arthrobacter ureafaciens* is highly purified and recognizes and cleaves at α(2→3)-, α(2→6)-, α(2→8)-, and α(2→9)-linked sialic acids (Sigma-Aldrich, 2020c). Enzymes that recognise multiple α-glycosidic bonds is a great tool when investigating unidentified glycans, and when it is not of interest to identify specific α-glycosidic bonds.

1.4 Bacterial adhesion

Bacteria are small, single-celled organisms that inhabit most environments on earth. Many bacteria colonize higher organisms and creates a symbiotic or commensal relationship with the host. The human gut microflora in the gastrointestinal tract is a good example of symbiosis. The microflora is shown to have multiple functions, as it participates in digestion, protects against pathogens, and affect the mucosal barrier (Wang *et al.*, 2017). Pathogens can also infect the host and cause disease. An imbalance between the host and the microflora is problematic and can turn beneficial bacteria parasitic.

In higher organisms, bacteria usually attach to the skin, and the mucosae associated with the respiratory tract, gastrointestinal tract and the urogenital system (Ribet and Cossart, 2015). To successfully colonize their target surface, bacteria depend on being able to somehow interact with and attach to their target host, and thus have developed a great number of mechanisms to do so. Bacterial adhesion often also promotes surface conditioning, which permanently alters the surfaces properties (Dunne, 2002).

Bacterial adhesion can be divided into the primary non-specific adhesion stage, and the secondary specific stage (Dunne, 2002). To initiate the primary stage, the bacteria must somehow be situated close to the surface, either by a natural flow or by forced placement. The cell-exterior is usually negatively charged, and electrostatic interactions favour repulsion between the bacteria and host cells. When the bacteria are located at the critical proximity of <1 nm from the host surface, the net sum of the weak, non-specific attractive and repulsive forces such as electrostatic, hydrophobic and van der Waals forces determines adhesion (Dunne, 2002). This interaction is also reversible. In the secondary stage, external molecules on the bacterial surface binds to structures on the host surface and thus form irreversible strong specific interactions.

1.4.1 Bacterial adhesion to target surfaces and mucins

Bacterial adhesion to the host surface depends on surface molecules that recognize and adhere to structures on the target surface. Many bacteria express adhesins, a surface molecule that mediates adherence. There are different types of adhesins, with different composition and potential to recognize various targets, some engaging in weak nonspecific interactions with the host, others in specific interactions with host receptors (Stones and Krachler, 2016). Many bacteria express appendages such as pili and fimbriae, and these often possess a great amount of adhesins (Formosa-Dague *et al.*, 2018). The associated adhesin of the bacteria allows target specificity, thus facilitating specific binding to the precise target surface. The most common adhesin found in bacteria are lectins, which are carbohydrate-binding proteins (Berg, Tymoczko and Stryer, 2002). They recognise and attach to glycans on cell surfaces. Each single lectin-carbohydrate interaction is weak, but multiple single interactions cause multivalency and increase the total binding strength. This is also known as the Velcro principle (Berg, Tymoczko and Stryer, 2002).

Many bacteria interact with the host mucus layer. The heavily glycosylated mucins in the mucus is a popular target among bacteria, and they also serve as a carbon and energy source (Sicard *et al.*, 2017). Bacteria can bind to mucins via specific lectins, but some bacteria also express mucus-binding proteins (MUB). The gut microbiota inhabits the mucosal layer covering the gut epithelium and is shown to regulate mucus composition and mucus secretion, but many pathogens have also developed mechanisms to attach to and manipulate the mucosal layer (Sicard *et al.*, 2017).

Bacteria also adhere to the host by glycan-glycan interactions. The cell surface of both bacteria and mammals express glycans to a great extent. Glycan-glycan interactions are defined as low-affinity weak interactions, and are considered a precede step prior to high-affinity interactions (Formosa-Dague *et al.*, 2018).

1.4.2 Biofilms

Bacterial colonies often produce biofilms once they are irreversibly attached to the target surface. The purpose of biofilms is to increase attachment and enclose the bacteria to the host surface. The film prevents dehydration, and protects the bacteria against predators, biocides, and other menaces (Dunne, 2002). Components in the biofilm are bacterial exopolysaccharides, along with components originating from the host such as proteins, nucleic acids, and nutrients. The glycocalyx also keeps the biofilm attached to the colonized surface (Dunne, 2002).

The formation of biofilms can be hard to prevent or remove once developed, and biofilms of parasitic microbes can cause great harm to the host. The host mucosal barrier does however play a crucial part in protecting the epithelial surface, and prevent direct bacterial contact with the host tissue (Caldara *et al.*, 2012).

1.4.3 *Arthrobacter* and *Janthinobacterium*

Arthrobacter

Most species of the genus *Arthrobacter* are obligate aerobic and gram-positive bacteria, and their genomes are composed of a high GC content (Fu *et al.*, 2014). The genus is chemoorganotrophic and can use various organic material as carbon and energy source (Eschbach *et al.*, 2003). *Arthrobacter* belongs to the *Actinobacteria* phylum and are abundant in soil, but they have also been isolated from other environments, such as fresh water, air, sludge, and even human skin (Fu *et al.*, 2014). Many species also produce biofilms (Dey and Paul, 2018). Their adaptability and properties makes them desirable in agriculture, medicine, and industry (Fu *et al.*, 2014).

Janthinobacterium

The *Janthinobacterium* genus belongs to the *Proteobacteria* phylum. Species are usually rod shaped, gram-negative aerobes, and they are chemoorganotrophs (Gillis and Logan, 2015). *Janthinobacterium* are usually found in soil and aqueous environments (Haack *et al.*, 2016). Many species produce biofilms, such as the species *Janthinobacterium lividum*. *J. lividum* is gram-negative and rod-shaped, and usually isolated from soil (Pantanella *et al.*, 2007; Oh *et al.*, 2019). Like some other strains, *Janthinobacterium lividum* also produce a purple pigment called violacein. The pigment has antibacterial, antiviral, and antifungal properties, and thus function as protection against environmental dangers for both the bacteria and the host (Oh *et al.*, 2019).

2. Experimental methods

2.1 Atomic force microscopy (AFM)

Atomic force microscopy is a high-resolution imaging technique that provides an image based on contact. It differs from traditional optical microscopy methods as it does not magnify the sample with lenses and a light source, but rather measure the force applied to the system (Dufrêne, 2017). The principle of the technique is that a sharp tip scans over a target surface, and interactions between the tip and surface is being monitored (Dufrêne and Hinterdorfer, 2008). The simple basics of the microscopy technique make it ideal for various applications in different fields as it can be used to study the topography of a wide range of both hard and softer samples. It can study smoothness and softness, but also investigate the interaction strength between single molecules (Kasas and Dietler, 2017). The resolution of AFM allows imaging of objects at the nanometer scale (Chang *et al.*, 2012).

The AFM is a simple microscopy method to use. A great advantage of the method is the simple preparation steps of the samples prior to measurements, which greatly reduce preparation time. The sample does not require any staining, labelling, or fixation (Dufrêne, 2017). AFM also allows measurements in aqueous solutions, which thus allows analysis of specimen close to their native environment (Chang *et al.*, 2012). The simple preparation step also makes it possible to analyse live cells, rendering the AFM an outstanding measurement device for analysing bacteria and bacterial adhesion. These features also render this microscopy technique one of a kind, and in high demand in many other fields.

The AFM exploits the interaction force between a probe, also known as a cantilever, and a surface, to gain information used for imaging (Chang *et al.*, 2012). By employing force spectroscopy, specific specimen properties can be analysed instead of topography. Various substrates can be attaches onto the probe, and interaction with their interacting counterpart prepared onto a surface can be measured. The position of the probe is continuously monitored by a laser focused onto the cantilever during calibration of the AFM, as illustrated in Figure 2.1. The laser beam is reflected onto a photodiode, which continuously monitors the laser. As the probe is lowered onto and retracted from the surface, the cantilever deflects, and the affected laser will be detected by the photodiode.

2.1.1 AFM components

Piezoelectric scanner

The piezoelectric scanner ensures a precise tip-to-sample placement and is controlled by a feedback loop. The piezoelectric scanner is a transducer that converts electrical potential into mechanical motion, and it expands or contract depending on the voltage of the applied electrical field (Eaton and West, 2010). The scanner used in AFM are usually an x-y-z scanner, which moves laterally (x and y) but also up and down (z). The z piezo scanner usually has a dynamic range of up to 10 microns, and a high resolution of <0.5 nm (Eaton and West, 2010). A z-stepper motor is also incorporated together with the z scanner to ensures a swift and accurate approach (Eaton and West, 2010).

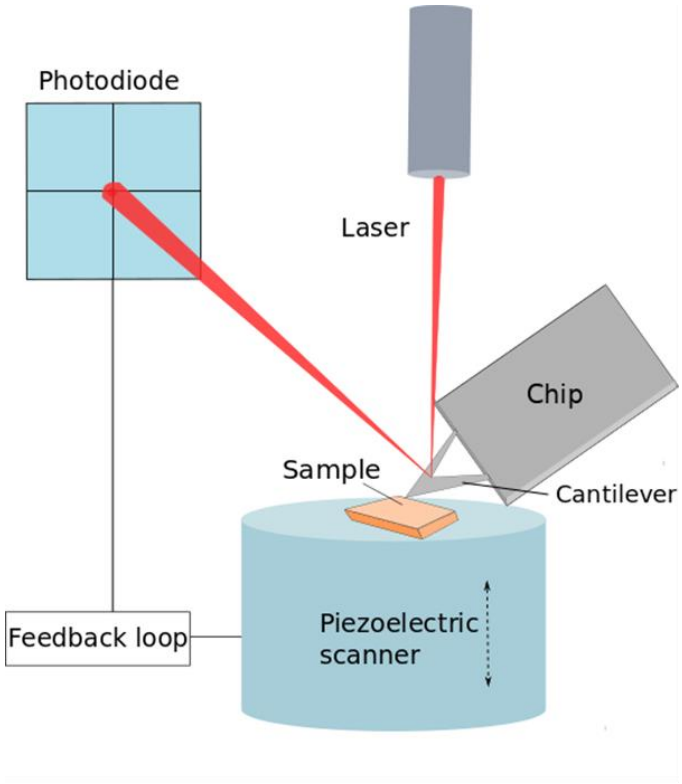

Figure 2.1: The basics of atomic force microscopy. A laser is focused onto the cantilever which scans the sample. Deflection of the laser is detected by a photodiode, which signals to the piezoelectric scanner through a feedback loop. Figure modified from (Ølnes, 2019).

AFM instruments can be divided into sample-scanning or probe-scanning microscopes depending on which part of the microscope the piezoelectric scanner is mounted on. In sample-scanning AFM, the transducer is mounted to the sample, while the probe remains fixed. The opposite relation is valid for the probe-scanning AFM, where the probe is mounted to the transducer and the sample remains fixed (Eaton and West, 2010).

Photodiode

The photodiode continuously observes the laser beam reflected from the cantilever and can detect small changes as the cantilever deflects. If there is no deflection, the laser is focused at the centre of the photodiode (Butt *et al.*, 2005). Deflection leads to a positional change of the laser, and this information can be used to calculate the position of the cantilever.

Force sensor

The force sensor, or force transducer, measures the force applied onto the probe as it contacts the sample. The force sensor if often a cantilever, which can either be tip-less or have a tip attached underneath (Eaton and West, 2010). The cantilever is often V-shaped, which makes it sturdy during measurements. It consists of a spring, and when applied to the surface, the cantilever will slightly bend (Butt, Cappella and Kappl, 2005). A laser is focused onto the cantilever during calibration of the AFM and will deflected as the cantilever bends (Chang *et al.*, 2012). The deflected laser beams are thus registered by the photodiode. Some force sensors

can measure forces down to 10 piconewton between a probe and the sample (Eaton and West, 2010).

In experiments regarding single molecule interactions, it is possible to attach molecules and living cells onto the cantilever, and thus measure interactions with the sample. This allows investigation of molecular structures and biological functions and adhesion.

Feedback control

A feedback system sends signals between the force sensor and the piezoelectric scanner and secure the correct placement of the probe in relation to the sample. The system ensures that the force applied to the probe is constant (Dufrêne and Hinterdorfer, 2008). When the probe contacts the sample and the applied force in increased, the piezoelectric scanner is informed via the feedback control, and retract the probe away from the sample (Eaton and West, 2010).

2.1.2 Force spectroscopy

Force spectroscopy is used in AFM to analyse specific specimen properties, such as molecular recognition, binding strength, and elasticity (Dufrêne, 2017). As AFM has a high resolution, specimens can be analysed with great accuracy. During measurements, cantilever deflection is measured as the cantilever is moved onto the surface and then retracted repeatedly to obtain multiple measurements. The measurement takes place at the same location, but the tip can be manually moved onto other sections of the sample to perform repetitive measurements on a larger part of the sample.

The relationship between the force applied to the surface and the cantilever deflection is determined by Hooke's law

$$F = -kd$$

where force (F) is determined by the spring constant (k) and the deflection (d) of the cantilever. Therefore, each individual cantilever must be calibrated prior to measurements to find their belonging deflection sensitivity (nm/V) and spring constant (N/m) (Hinterdorfer and Dufrêne, 2006).

Measurement with force spectroscopy exhibit each specimen interaction in force curves (Figure 2.2), where the x-axis presents the cantilever positional height, and the y-axis shows deflection (Dufrêne, 2017). The cantilever approaches the sample and form weak interaction with the surface. This cause downward bending of the cantilever and thus a contact jump (Figure 2.2b) when the attractive forces are stronger than the repulsive forces and the spring constant (Butt, Cappella and Kappl, 2005). As the probe have contacted the sample, it can approach further into the sample to measure the surface softness by the repulsive force (Figure 2.2c). As the force reach a set value, the cantilever is retracted, and the repulsive force is released. As the cantilever retracts, present interaction between the probe and sample also cause a downward bend of the cantilever, which is represented as hysteresis (Figure 2.2d). This illustrate the force required to separate the interaction (Hinterdorfer and Dufrêne, 2006).

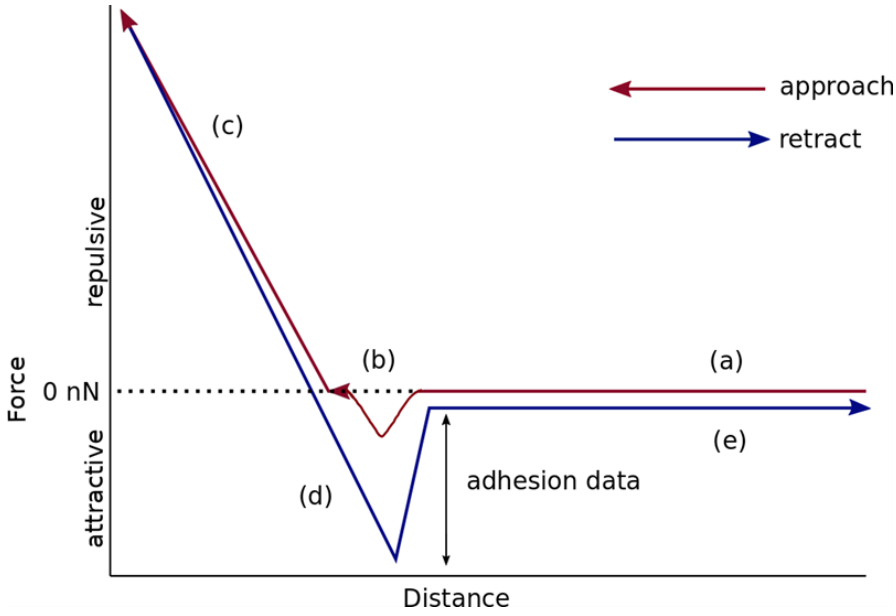

Figure 2.2: AFM force curve displayed as distance or height of the probe in relation to the applied force. The force curve represents approach (red) and retraction (blue). The cantilever is moved against the sample (a) and is subject to a contact jump (b). The tip is dived further into the sample, and the repulsive force is increased (c). The probe is retracted, the repulsive forces is released, and rupture force is measured (d). Figure modified from (Erdal, 2019).

2.2 Fluorescence microscopy

Fluorescence microscopy is a widely used optical microscopy technique that is based on imaging of specimens containing fluorescent dyes (Zhang and Hoshino, 2019). It differs from normal light microscopy as the light source emits light that cause photoluminescence of fluorophores in the sample. Specimens analysed with fluorescens microscopy must possess fluorescent molecules (fluorophores), which are molecules that can absorb photons and re-emit light. When fluorophores absorb energy of a given wavelength, an electron is exited. The electron is not stable in this position, and the energy will be lost as the electron returns to the ground state. (Sanderson *et al.*, 2014). The emitted light can then be observed in a fluorescent microscope. The downside of using fluorophores as dyes is that they are sensitive to light and will usually undergo photobleaching (Sanderson *et al.*, 2014). They will also slowly fade as they are being analysed by a fluorescent microscope. Samples are hard to store intact after they are stained, and they often need to be analysed shortly after treatment. The dyes also need to be stored as dark as possible prior to staining.

Fluorescence microscopy is a popular and frequently used imaging technique in many laboratories worldwide. There is a considerable amount of available fluorescent labels on the market, with different excitation spectra and ability to stain a distinct target molecule or molecular structure. This staining method is favourable as it is easy to use, and multiple stains can be used on the same sample at the same time to stain and visualise various components (Sanderson *et al.*, 2014). There is a great demand of fluorescent proteins, and a great business has been developed for producing and providing these proteins. Several methods for attaching fluorophores onto the specimen have also been developed. To stain specific structures, fluorophores can be attached onto antibodies, which then links to the molecule. This is also known as immunofluorescence, and is a great way to ensure target specificity (Zhang and Hoshino, 2019).

2.2.1 Components of the fluorescence microscope

In addition to a light source, the fluorescence microscope is composed of a dichroic mirror, an objective lens, excitation and emission filters, and a detector (Figure 2.3) (Zhang and Hoshino, 2019). The filters are adjusted and used to select the correct excitation and emission wavelength of the fluorophore applied to the specimen. The dichroic mirror is also disposed to ensure transfer of the target wavelength. This means that only one fluorophore can be examined at the time, even though a specimen can be stained with multiple fluorophores. However, photos of separate fluorophores can be merged later.

The properties of the objective lens used in fluorescence microscopy is also of great importance. It is preferred to use lenses with a high numerical aperture (NA), which is the objectives ability to gather light. This is of greater importance than the magnitude, as the NA helps resolve the specimen. A higher NA has a greater ability to distinguish adjacent objects (Lichtman and Conchello, 2005).

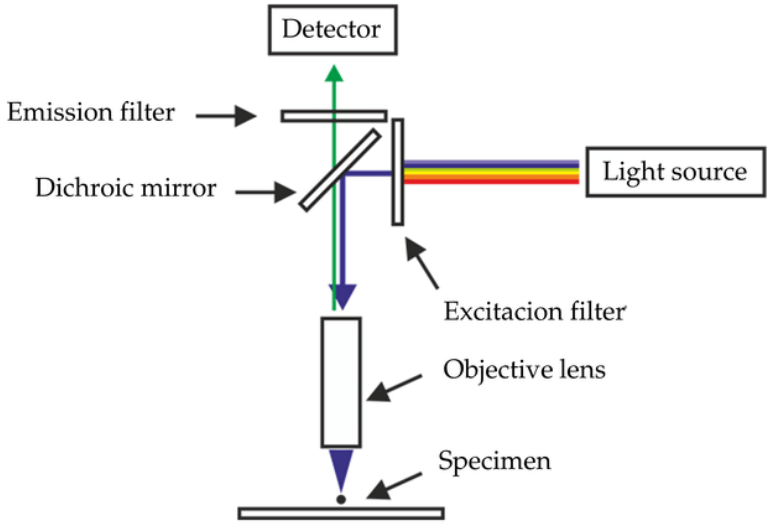

Figure 2.3: Components of the fluorescence microscope. Figure from (Majtner, 2015)

2.3 Immobilisation of bacteria and mucins

2.3.1 Polydopamine

Polydopamine (PDA) is a polymer with strong adhesive properties, and is commonly used as a tool to functionally immobilise molecules and whole cells onto a variety of target surfaces, both organic and inorganic (Tyo *et al.*, 2019). The interaction between the polydopamine and surface on which it is attached is caused by weak non-specific interactions, such as hydrophobic interactions, hydrogen bonds, cation-π interactions and π-π stacking (Zhang *et al.*, 2017). To coat any target surface, dopamine simply needs to be activated (oxidised) and applied, and thus allowed to polymerise. This makes them easy and desirable to use in various experiments.

The dopamine monomer is composed of a catechol (a benzene ring with two hydroxy groups) and an ethyl chain terminated with an amine group (Liu *et al.*, 2014). These functional groups can interact with multiple components and substrates. When exposed to alkaline conditions (pH > 7), the monomers are oxidized and undergo self-polymerization (Ding *et al.*, 2016). The molecule is also pigmented, and polymerisation cause a visible colour change, which develops further over time. The colour change can be used as an indication of polymerisation (Liu, Ai and Lu, 2014).

2.3.2 Silanes

Silanes are silicone-based chemicals used to enhance adhesion between organic and inorganic substrates (Pape, 2011). Organic and inorganic material usually possess different chemical and functional properties, and it can be hard to obtain strong adhesion between them. Most silane molecules are composed of a silicone atom attached to three inorganic hydrolysable groups, and one organic organofunctional group connected by a hydrocarbon chain (Pape, 2011). The hydrolysable groups are commonly alkoxy, methoxy and ethoxy.

Silanes can thus be used to attach organic specimen onto various surfaces. The hydrolysable part of the silanes is used to attach the molecule onto a target surface, and the organofunctional group will interact with the organic specimen. The organofunctional group is thus selected based on the specimen properties (Pape, 2011).

3. Materials and methods

3.1 List of chemicals

- Acetic acid, 1 mM HAc.
- Boric acid, 50 mM, pH 5.8 (Sigma Aldrich)
- Dopamine hydrochloride, polydopamine (PDA) (Sigma-Aldrich)
- EDC, N-(3-dimethylaminopropyl)-N'-ethylcarbodiimide hydrochloride, crystalline (Sigma-Aldrich)
- Mucin from bovine submaxillary glands (BSM), Type I-S (Sigma-Aldrich)
- Mucin from porcine stomach (PGM), Type III (Sigma-Aldrich)
- Neuraminidase, α(2→3,6,8,9) Neuraminidase from *Arthrobacter ureafaciens* (Sigma Aldrich)
- Neuraminidase 5X Reaction Buffer (Sigma Aldrich)
- Propidium iodide, 20 mM solved in DMSO, LIVE/DEAD Blacklight Bacterial Viability Kits (Molecular probes)
- Salmon gnotobiotic medium (SGM), (recipe: Appendix)
- Silane-COOH, N-[(3-Trimethoxysilyl)propyl] ethylenediamine triacetic acid trisodium salt (abcr GmbH)
- SYTO 9 dye, 3.34 mM solved in DMSO, LIVE/DEAD Blacklight Bacterial Viability Kits (Molecular Probes)
- Tris buffer, 10 mM, pH 8.5 (Sigma-Aldrich)
- Tryptic soy agar (TSA), containing tryptic soy broth and agar powder (Sigma-Aldrich) (recipe: Appendix)
- Tryptic soy broth (TSB) medium (VWR chemicals)

3.2 Bacterial immobilisation to AFM cantilever

3.2.1 Cultivation of bacteria

Bacterial strains from the genera *Arthrobacter* and the bacteria *Janthinobacterium lividum* was previously isolated from the skin of Atlantic salmon (*Salmo salar*) fry, genotyped, and preserved as glycerol stocks at -70 °C in Eppendorf tubes. In this thesis, bacteria were collected from the glycerine stock, plated onto tris soy agar (TSA) (see Appendix) plates, and left in room temperature until single colonies could be isolated (2-4 days). Each colony were transferred to 3 mL of tryptic soy broth (TSB) medium in sterile conditions and left in room temperature until the next day.

3.2.2 Immobilisation of *Janthinobacterium* and *Arthrobacter* to AFM cantilever

Janthinobacterium and *Arthrobacter* were immobilised onto tipless rectangular cantilevers (Nanoworld, PNP-TR-TL), by using a 4 mg/ml solution of polydopamine (PDA). The chips containing the cantilevers have two cantilevers on each side, one bigger than the other. They were treated together, but the bigger cantilever was used in measurements.

Each individual AFM probe was applied with 20 µl from a solution composed of 250 µl tris buffer mixed with 1 mg polydopamine hydrochloride. The tris buffer is alkaline and activates polymerisation of dopamine. PDA promotes strong interactions with substrates and is proven a reliable adhesion mediator. The treated probes were incubated in room temperature for 45 minutes then washed with milli-Q water. 20 µl of TBS solution containing bacteria were applied onto the probes in sterile conditions and incubated in room temperature until the next day, where they were washed with salmon gnotobiotic medium (SGM) prior to experimental measurements.

After two days of measuring bacterial adhesion to BSM and PGM, it was discovered that *Janthinobacterium* produced too much biofilm when isolated until the next day. When observed in a light microscope, the cantilevers were somehow bent or more fragile than they should be, and the cantilevers originally prepared for day 3 could not be used for AFM measurements. A test experiment was performed to see how much biofilm was produced after incubation for exactly 12 hours, and the production was high. The biofilm could not be washed away from the cantilevers, and the cantilever were bent. As of Day 3, the incubation time was reduced to 2 hours for all measurements performed with *Janthinobacterium*. A live/dead assay with the L7012 LIVE/DEAD® BacLight Bacterial Viability Kit (Molecular probes) and observation with the fluorescent microscope Zeiss Axio Observer.Z1 confirmed a sufficient bacterial density on the cantilever after 2 hours.

3.2.2 Live/dead assay of immobilized bacteria

Live/dead assays were performed on *Janthinobacterium* and *Arthrobacter* immobilised onto AFM cantilevers with PDA, to investigate the abundance of immobilized bacteria and the live-dead ratio. Probes with attached bacteria was treated with the L7012 LIVE/DEAD® BacLight Bacterial Viability Kit (Molecular probes). The kit uses two types of dye: SYTO 9 and propidium iodide. The SYTO 9 is a green dye that labels intact cells. Propidium iodide is a red dye that labels damaged membranes. The dye cannot cross the cell membrane of live cells.

The LIVE/DEAD staining was performed according to the manufacturer's description in the L7012 LIVE/DEAD BacLight Bacterial Viability Kit. A 1:1 mixture of SYTO 9 solution and propidium iodide solution (1,5 µl of each, collectively 3 µl) was added to 1 ml SGM media and applied onto the bacteria-coated cantilevers. They were incubated away from light for 20 minutes, the excess solution was removed, and the cantilever was washed with SGM.

The stained cantilevers were directly placed upside down on WillCo dishes (Ø 35 mm) and visualized with the fluorescent microscope Zeiss Axio Observer.Z1. The SYTO 9 stain and propidium iodide stained bacteria was visualized and depicted with the Syl9 and LDAqu filters.

3.3 Preparation of mucin-coated mica sheets

3.3.1 Immobilisation of BSM and PGM mucins on mica sheets

The mucins were attached to the mica sheets by EDC-catalysed coupling to silanes. To prepare the attachment of mucins onto the mica sheets, the sheets were cut to an appropriate size and cleaved into two with tweezers. 6 µl silane-COOH were mixed with 494 µl acetic acid, and 250 µl of the solution weas applied onto each square. They were incubated in room temperature for 20 minutes, the excess solution was removed, and the sheets were washed with acetic acid.

The mucins were prepared with EDC (N-(3-dimethylaminopropyl)-N'-ethylcarbodiimide hydrochloride), a coupling agent that links amino groups and carboxyl groups together. In mucin attachment, EDC mediates the covalent binding between the silane on the mica sheet, and the mucin. 1 mg EDC was mixed with 500 µl boric acid, and 250 µl of the solution were applied to each 0.25 mg of bovine submaxillary mucin (BSM) and porcine gastric mucin (PGM) and incubated in room temperature for 1,5 hours. The excess media was removed, and the sheets was glued onto the bottom of small glass Petri dishes with JPK glue, and left to dry for 15 min. The glue was empty after experiments of Day 2 and were switched with superglue as of Day 3. The dishes were then filled with SGM until the sheets were completely covered.

3.3.2 Neuraminidase treatment of BSM and PGM

As many bacteria interact with host glycans and sialic acids, it was of great interest to see how bacterial adhesion would be affected by treating the mucins with neuraminidase. BSM and PGM was prepared onto mica sheets as previously described, and then additionally treated with neuraminidase. $\alpha(2\rightarrow3,6,8,9)$ neuraminidase from *Arthrobacter ureafaciens* was prepared according to manufacturer's instructions and 4 units of active enzyme was added to each mucin-coated surface, dissolved in a 50 µl solution. The mixture was used within 7 days after preparation. The sheets were incubated at 37°C for 30 minutes, and then washed with SGM.

3.4 AFM measurements of bacterial adhesion to mucins

The two types of experiments performed in this thesis was measurements of bacterial adhesion to BSM and PGM, and BSM and PGM treated with neuraminidase. All AFM measurements in this thesis were performed with force spectroscopy using the JPK Force Robot 300, and tipless cantilevers (Nanoworld). The cantilevers with immobilised bacteria were mounted on the probe-scanning AFM head. Prior to measurements, each cantilever was brought in contact with a clean glass surface to determine the detector sensitivity. Additionally, the spring constant of

the cantilever was determined based on its thermal fluctuation. After calibration, the clean glass surface was swapped with a glass slide containing the mucin coated mica sheets in 3 ml SGM. The AFM head was placed on top of the glass slide, and the AFM cantilever was lowered into the aqueous solution and applied onto the mica sheet. Most of the AFM default settings were used during the measurements, but the retraction delay was set to 0,2. The Z length was usually set on 1.0 but could occasionally be adjusted to 2.0 depending on background noise. During measurements on mucins treated with neuraminidase, the Z length usually had to be set higher (2.0-5.0).

Between 600 and 1200 measurements were performed on each mica sheet for each measurement day, usually covering 3-5 different areas on the surface. This resulted in an equal number of force-distance curves for each mucin. Measurements of bacterial adhesion between *Janthinobacterium* and *Arthrobacter* onto both BSM and PGM was performed 4 to 5 times, and the different experimental series were names Day 1-5. Measurements on BSM and PGM treated with neuraminidase was performed 5 times, named Day 1-5. A new cantilever with coated bacteria, and new mica sheets were prepared and used for each measurement day. The same probe was used on the same day for the same bacteria on both mucins measured that day, but none of the probes were used multiple days. It was important to use new bacteria and mucins each day to ensure independent data.

3.4.1 Analysis of AFM force curves

The force-distance curves were processed with the JPK Processing software. Curves lacking any visible interaction was discarded, and curves with visible interactions were processed. Interactions could be seen where the curved stretched beneath the baseline, which constitute the deadhesion work (see Figure 2.2). This area was measured, and the data was saved as text files. The processed text files were transferred to SigmaPlot to prepare histograms showing the frequency of magnitudes of the deadhesion work. Histograms from each experimental day of the same bacteria interacting with the same mucin were prepared and compared.

SigmaPlot was also used to prepare galleries presenting some of the most common force-distance curves, with text files prepared with Interactive Data Language (IDL). With the IDL Data Visualization Software (DiForDisMultiJPK3), the chosen force-distance curves were presented next to each other to represent the common interaction patterns.

To further investigate the adhesion strength of single molecular interactions based on the force-distance curves, the IDL version difordisjpkv31dr3 was used to determine the rupture force. The processed data was transferred to SigmaPlot to make scatter plots of the rupture force plotted against the loading rate, and histograms showing the rupture force distribution.

4. Results

The objective of this thesis was to investigate and compare the adhesive properties of *Janthinobacterium* and *Arthrobacter* to bovine submaxillary glands (BSM) and porcine gastric mucin (PGM), both untreated and treated with neuraminidase. Some methods were optimized during the experiment, and viability of bacteria immobilized on the cantilever was controlled with live/dead assay.

4.1 Bacterial immobilisation to AFM cantilever

4.1.1 Cultivation of bacteria

Arthrobacter required a longer cultivation time than *Janthinobacterium*, both on the TSA plates and in the TSB media. *Arthrobacter* could usually cultivate on TSA plates for 4-5 days before it was possible to isolate single colonies, which were transferred to TSB media and incubated for 1-2 days. Single colonies of *Janthinobacterium* could usually be isolated from TSA plates after 2-3 days, and transferred to TSB media, where a synthesised biofilm was visible simply after one day. *Janthinobacterium* isolated in TSB media for two days produced an excessive amount of biofilm, and it was problematic to avoid transfer of biofilm along with the bacteria onto AFM cantilevers.

4.1.2 Immobilisation of *Janthinobacterium* and *Arthrobacter* to AFM cantilever

Bacteria were immobilised on the AFM cantilever with polydopamine (PDA). Both bacteria strains were incubated on the polydopamine-treated cantilevers until the next day, but the incubation time for *Janthinobacterium* was reduced to two hours due to weakened cantilevers. When *Janthinobacterium* was isolated on the cantilever for 12-24 hours, bent cantilevers could be observed with light microscopy.

4.1.3 Live/dead assay of immobilized bacteria

Live/dead assay was performed on *Janthinobacterium* and *Arthrobacter* immobilized onto tipless cantilevers to validate viability. Once the probes were stained, they could no longer be used for experimental measurements with AFM. Therefore, unused probes treated with bacteria were stained and compared to the used probes.

It was discovered that probes isolated with *Janthinobacterium* for 12-24 hours were destroyed, and they could not be used in measurements. Analysis with light microscopy showed that many cantilevers were bent at the base, and supposedly intact cantilevers would bend when lowered into an aqueous phase during AFM calibration. An experiment was performed where *Janthinobacterium* was incubated onto AFM probes treated with PDA for 12 hours, then stained and visualized with fluorescent microscopy (Figure 4.1).

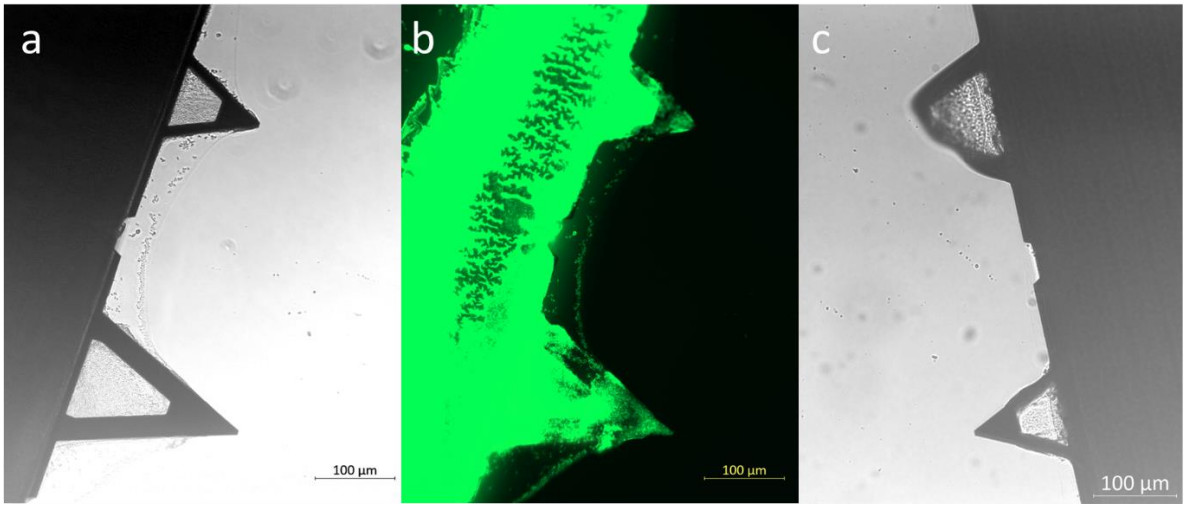

Figure 4.1: Viability of *Janthinobacterium* after incubated onto AFM cantilevers for 12 hours. 4.1a and b presents the same probe, visualised in phase contrast (4.1a) and with fluorescent microscopy (4.1b). Figure 4.1c illustrates a bent cantilever visualised using phase contrast microscopy.

Figure 4.1 reveal a high density of immobilised bacteria and what appears to be a large amount of biofilm on the cantilevers. The rectangular cantilevers are coated with a gel-like material, and in Figure 4.1a and b bacteria is distributed within the gel-like material connecting the cantilevers.

Due to the problematic amount and effects of the bacteria and the gel-like material produced by the bacteria, the incubation time of *Janthinobacterium* was reduced to 2 hours. The viability of the bacteria immobilised using the modified approach is represented in Figure 4.2. The viability of *Janthinobacterium* isolated on cantilevers for 2 hours gave a sufficient density of bacteria (Figure 4.2a), and none of the cantilevers were seen to bend or break after treatment.

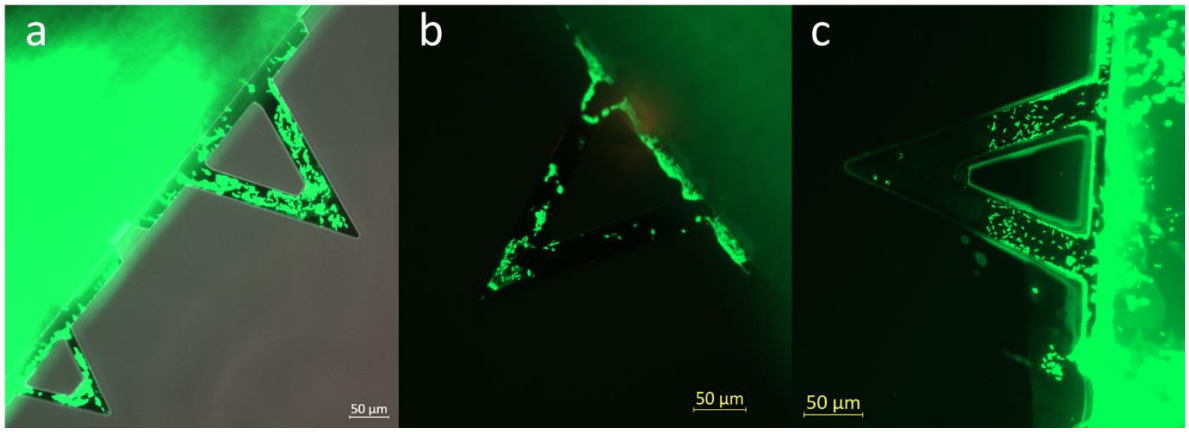

Figure 4.2: Viability of *Janthinobacterium* after incubation onto AFM cantilevers for 2 hours. The images depict cantilever not used for measurements (a) and cantilevers used for measurements on Day 4 of the experiments performed as part of the method-development b), and on Day 1 of the neuraminidase-experiment (c). The unused cantilever was included to enable a comparison between used and unused cantilevers. The bacterial density on the used tips (b and c) is lower than on the unused tip (a).

The incubation time of *Arthrobacter* immobilization was kept at ~ 24 hours for all experiments, as the cantilevers did not seem to be adversely affected by the long incubation time. As *Arthrobacter* required a longer cultivation time on the TSA plates and in the TBS media than *Janthinobacterium*, it was believed that they also required a longer incubation time on the cantilevers. Arthrobacter viability is revealed by images obtained after live/dead staining presented in Figure 4.3.

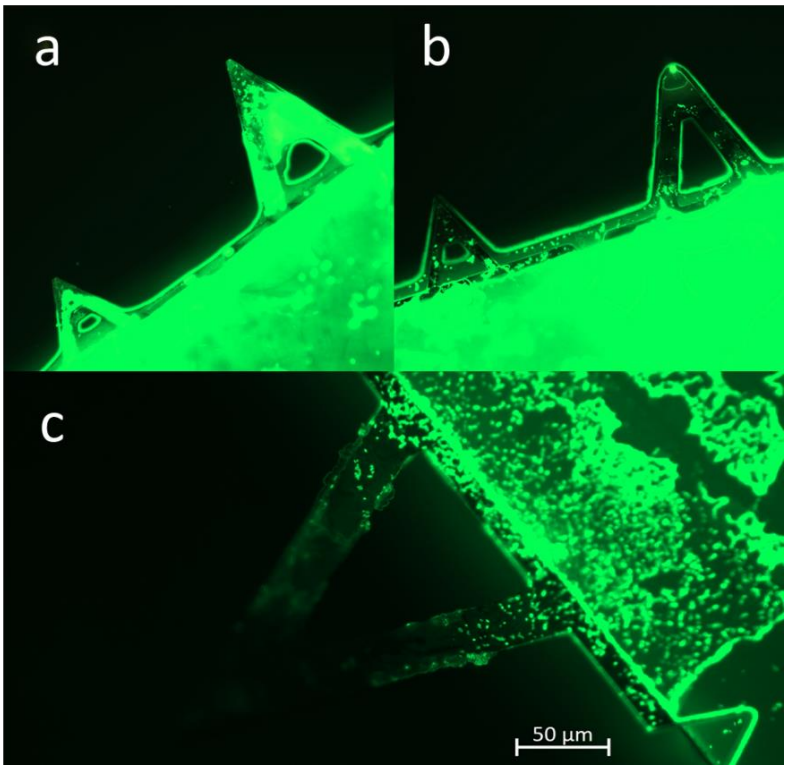

Figure 4.3: Viability of *Arthrobacter* after incubation onto AFM cantilevers for ~ 24 hours. The images are obtained when inspecting an unused cantilever (a) and used cantilevers in experiments on Day 2 of the neuraminidase-experiment (b), and Day 4 of the method-development experiment (c).

Both Figure 4.2b and c, and Figure 4.3b and c, reveal the viability of bacteria on the probes that have been used in the experiments, and the density of the bacteria is clearly lower than that of the corresponding cantilevers not used for experiments. The bacterial density on the cantilevers on Figure 4.2c and Figure 4.3c is lower on the tip than on the cantilever legs.

All stained cantilevers, both unused and used in measurements, is mainly coloured green, and only a weak hint of red is shown in some of the images. This indicates good bacterial viability, and that the immobilized bacteria used in experiments has remained alive throughout the measurements.

4.2 AFM measurements of bacterial adhesion to mucins

4.2.1 Bacterial adhesion to BSM and PGM

Measurements of bacterial adhesion of *Janthinobacterium* and *Arthrobacter* to both BSM and PGM were performed between 4 and 5 times to each mucin, and bacterial adhesion to BSM and PGM treated with neuraminidase was performed 5 times to each mucin. The measurements are presented as individual days in Figure 4.4 and Figure 4.5.

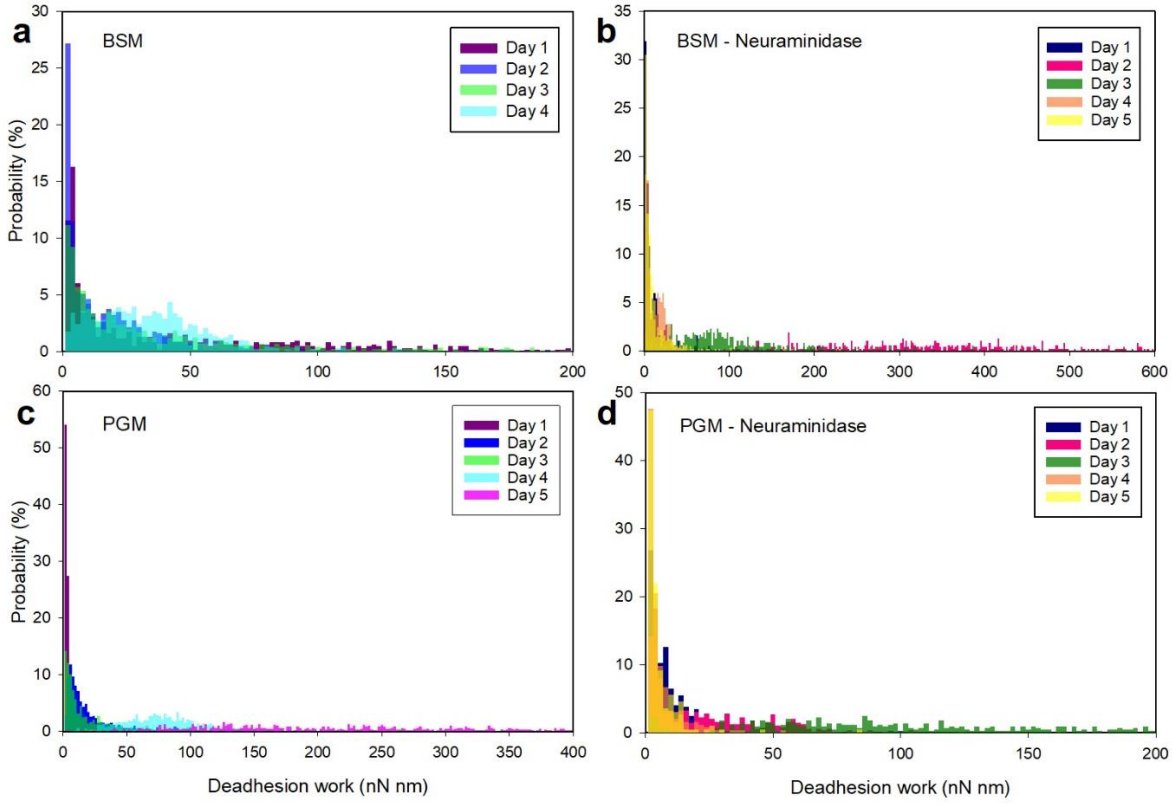

Figure 4.4: Histograms showing the magnitude of the deadhesion work (nN nm) quantified between *Arthrobacter* and BSM (a) and BSM treated with neuraminidase (b), and PGM (c) and PGM treated with neuraminidase (d). The same probe was used on the same measurement days for a) and c), and b) and d), and these experimental series are therefore presented with identical colours.

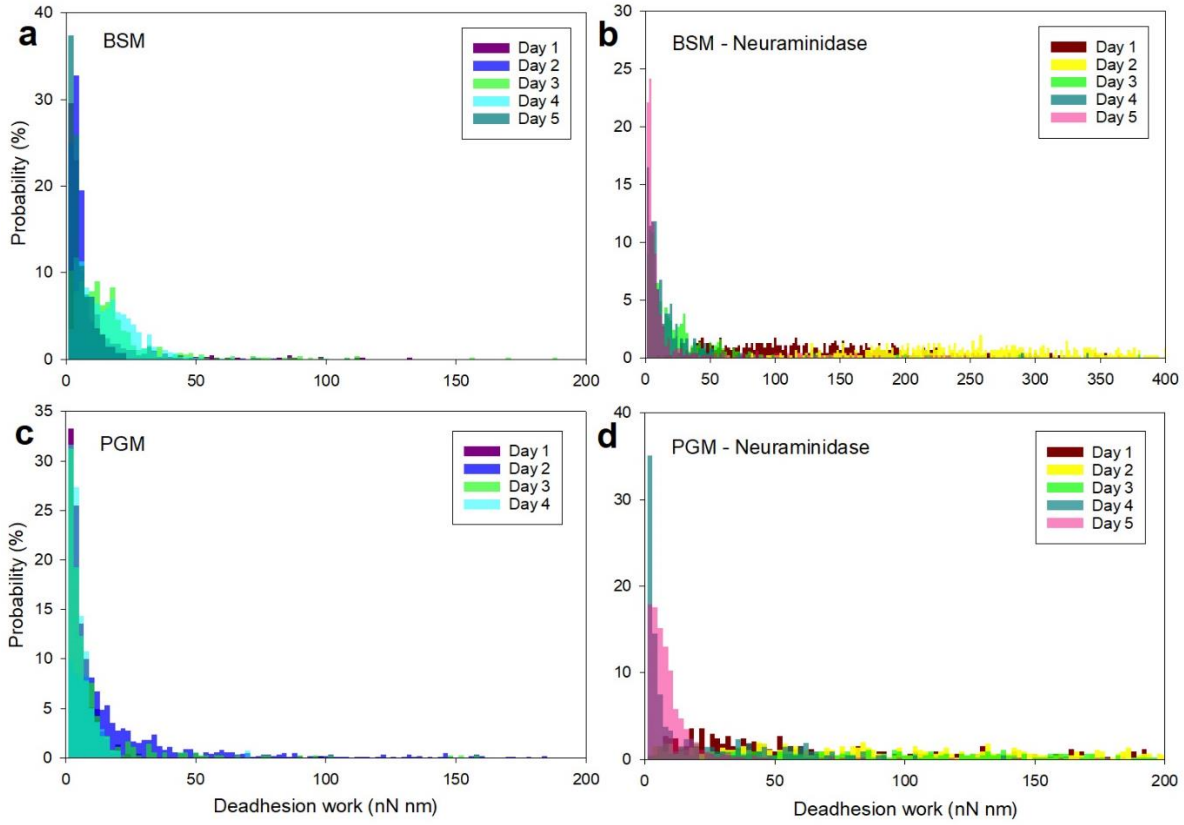

Figure 4.5: Histograms showing the magnitude of deadhesion work (nN nm) quantified between *Janthinobacterium* and BSM (a) and BSM treated with neuraminidase (b), and PGM (c) and PGM treated with neuraminidase (d). The same probe was used on the same measurement days for a) and c), and b) and d), and these experimental series are therefore presented with identical colours.

4.3.2 Comparison of bacterial adhesion and force curves

In order to compare the bacterial adhesion to BSM and PGM, and BSM and PGM treated with neuraminidase, common force curves of each bacterial interaction was prepared in SigmaPlot and supplemented to the histograms of each bacteria to each mucin (Figure 4.6 and 4.7).

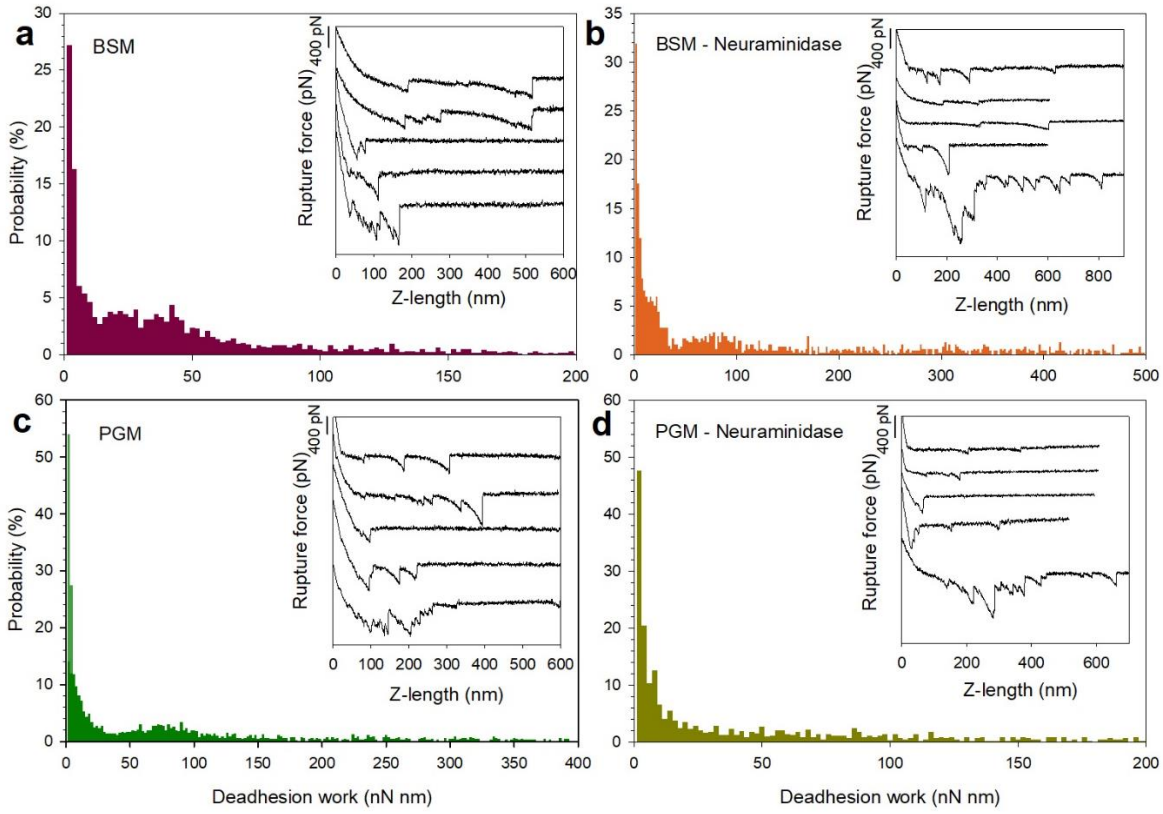

Figure 4.6: Histograms showing the magnitude of deadhesion work (nN nm) between *Arthrobacter* and BSM (a) and BSM treated with neuraminidase (b), and PGM (c) and PGM treated with neuraminidase (d). Five common force-distance curves were chosen for each mucin, plotted as Z-length (nm) in relation to rupture force (pN).

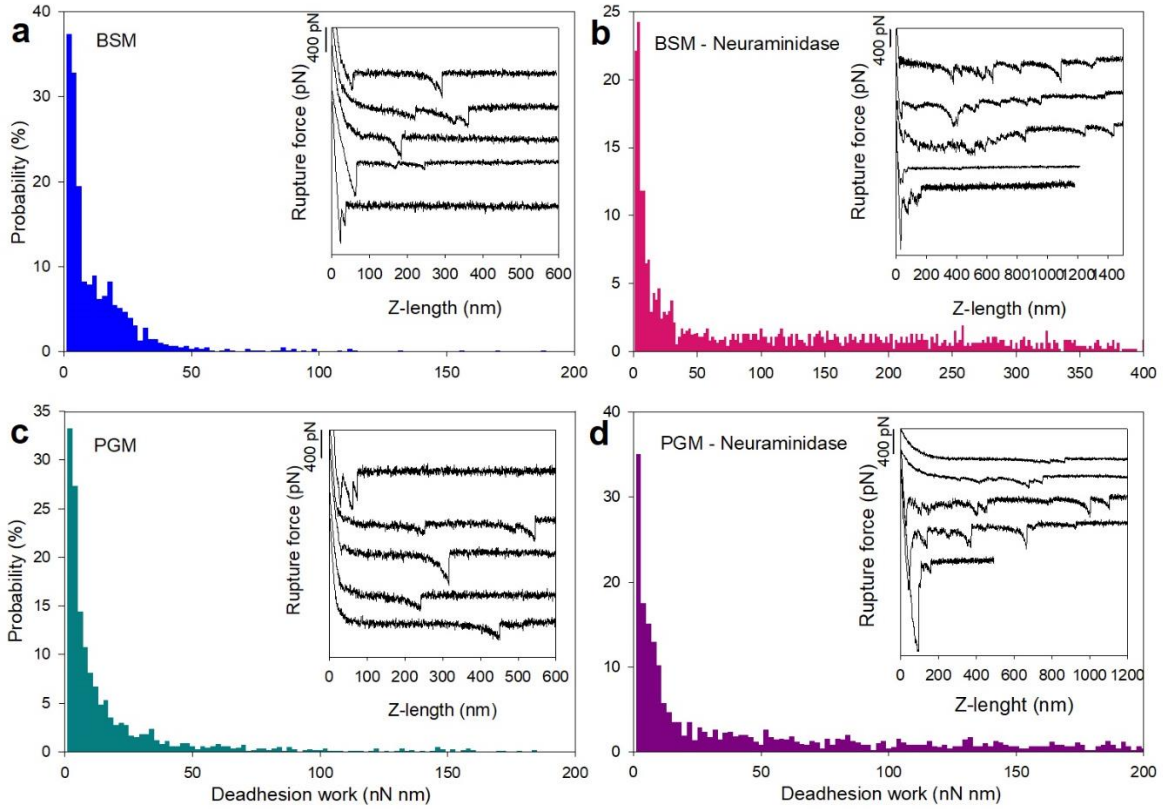

Figure 4.7: Histograms showing the magnitude of deadhesion work (nN nm) between *Janthinobacterium* and BSM (a) and BSM treated with neuraminidase (b), and PGM (c) and PGM treated with neuraminidase (d). Five common force-distance curves were chosen for each mucin, plotted as Z-length (nm) in relation to rupture force (pN).

4.3.3 Analysis of single molecular pair interactions

In addition to analysing the total amount of bacterial adhesion of *Janthinobacterium* and *Arthrobacter* to BSM and PGM, it was of interest to analyse the binding strength of single molecular pair interactions. Scatter plots (Figure 4.8 and 4.10) and histograms (Figure 4.9 and 4.11) were prepared from IDL data where distinct interactions were chosen and included in the dataset. Many force curves were discarded, as they possessed multiple interactions, and simple well-separated interaction peaks could not be identified.

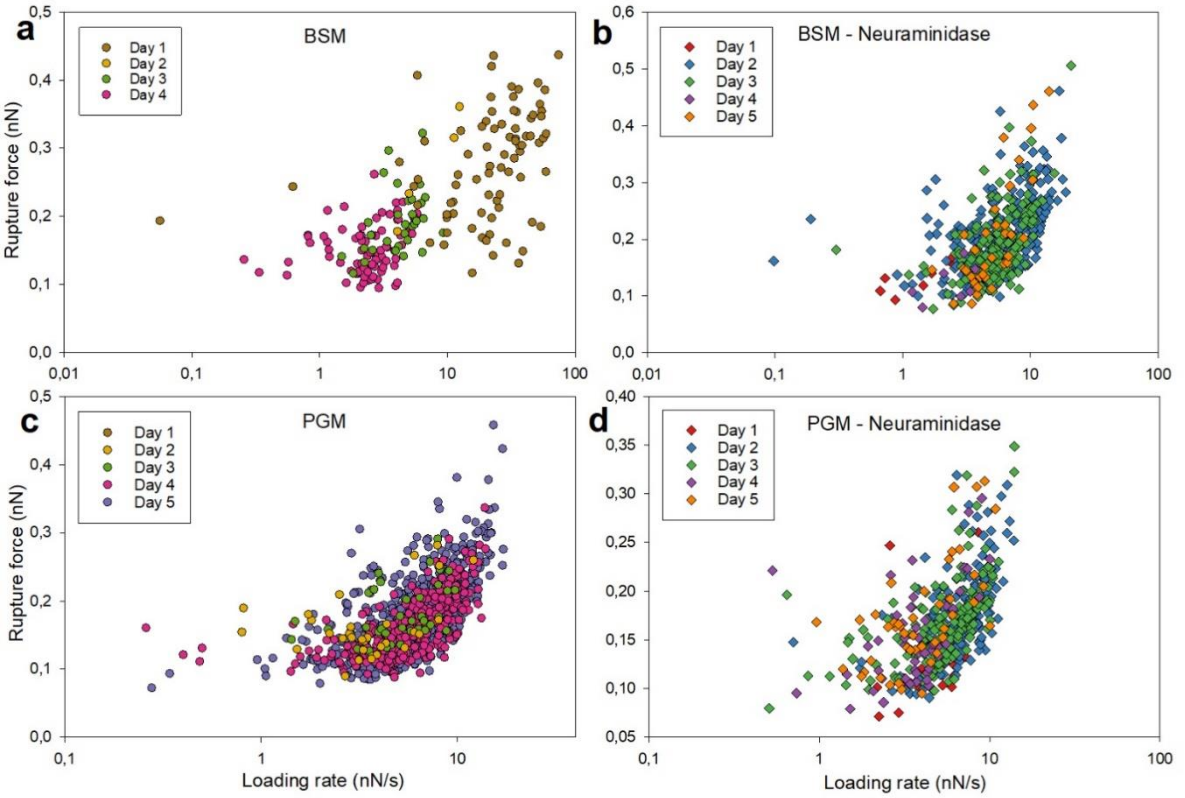

Figure 4.8: Scatter plots showing the rupture force (nN) as a function of loading rate (nN/s) for the interaction between *Arthrobacter* and BSM (a) and BSM treated with neuraminidase (b), and PGM (c) and PGM treated with neuraminidase (d).

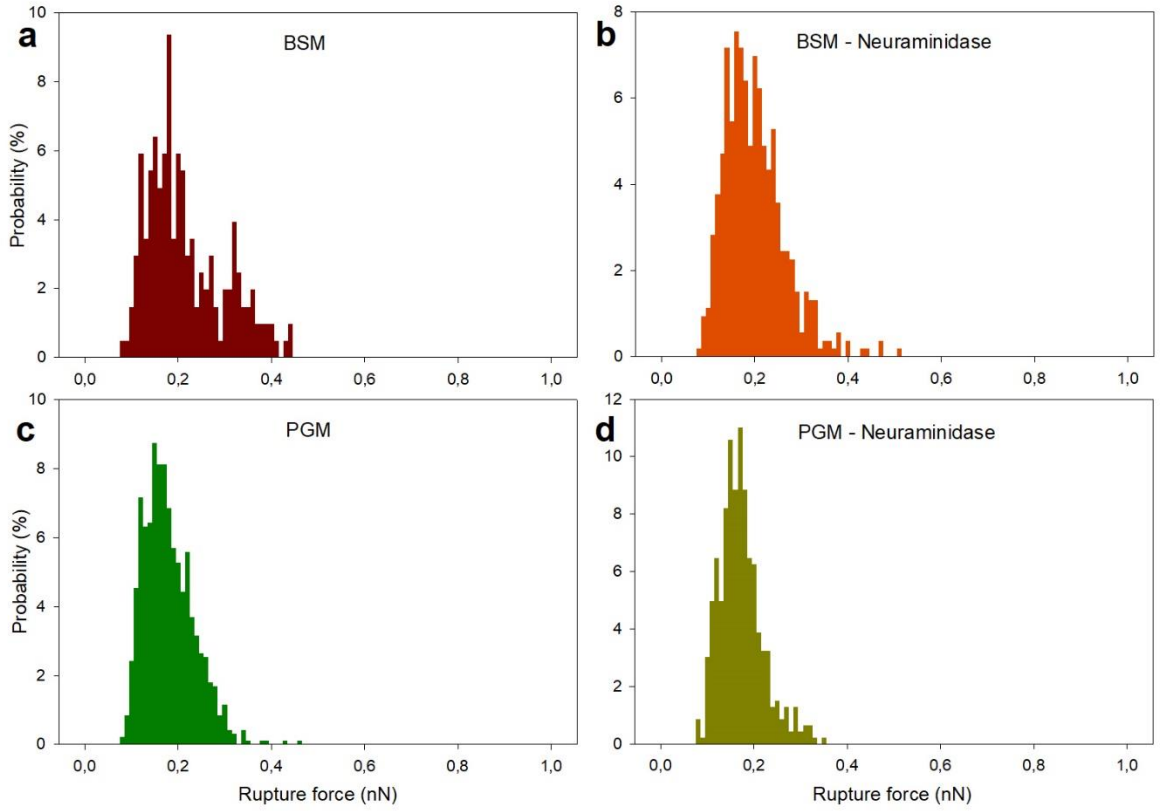

Figure 4.9: Histograms showing the distribution of rupture forces (nN) of single molecular bond interactions between *Arthrobacter* and BSM (a) and BSM treated with neuraminidase (b), and PGM (c) and PGM treated with neuraminidase (d).

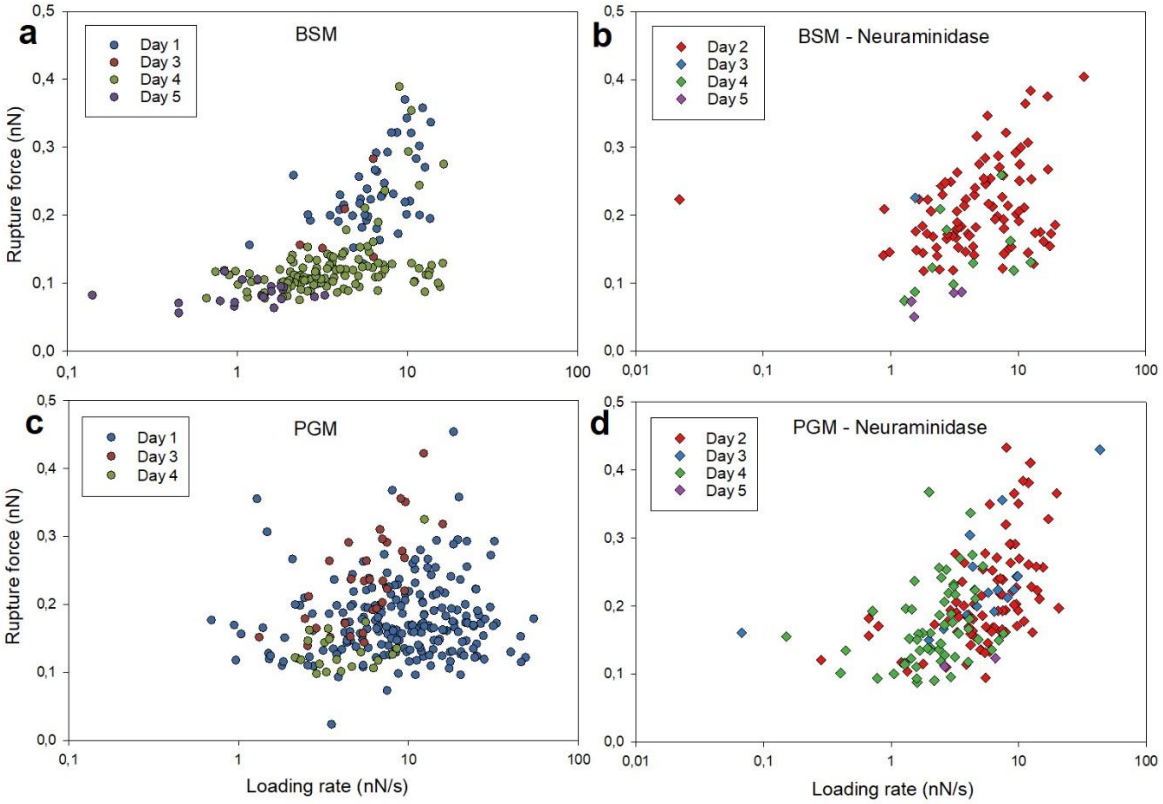

Figure 4.10: Scatter plots showing the rupture force (nN) as a function of loading rate (nN/s) between *Janthinobacterium* and BSM (a) and BSM treated with neuraminidase (b), and PGM (c) and PGM treated with neuraminidase (d).

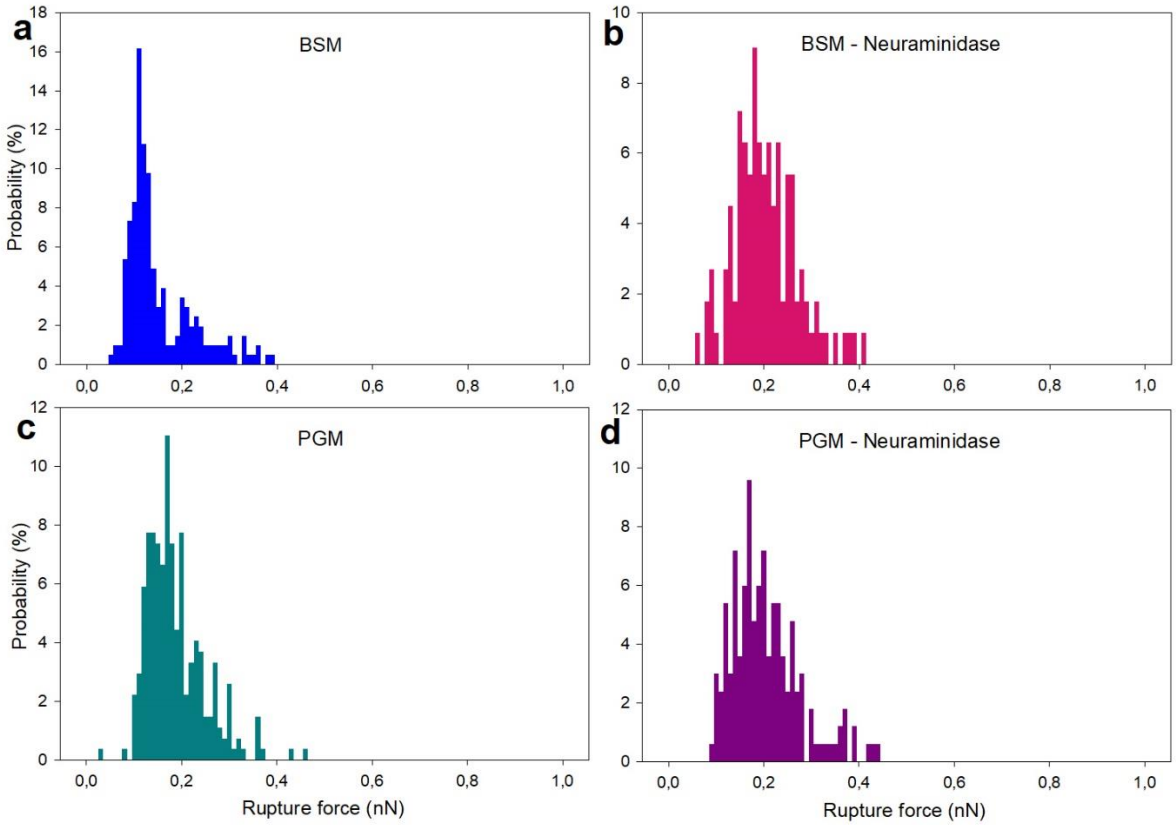

Figure 4.11: Histograms showing the distribution of rupture forces (nN) of single molecular bond interactions between *Janthinobacterium* and BSM (a) and BSM treated with neuraminidase (b), and PGM (c) and PGM treated with neuraminidase (d).

5. Discussion

5.1 Bacterial immobilisation to AFM cantilever

The live/dead assay performed of immobilized *Janthinobacterium* and *Arthrobacter* indicated a high viability of the bacteria. The stained bacteria were green, and no red bacteria were detected throughout the experiment. The bacterial density on the cantilevers also indicates that treatment with PDA does promote bacterial mobilisation on the AFM probes even though a complete coverage is not obtained. The live/dead assay indicated that bacteria were indeed attached onto the probe.

The incubation time for *Janthinobacterium* was reduced to 2 hours, as the cantilevers kept in contact with bacteria for 12-24 hours would bend and thus be unsuited for AFM measurements. As presented in Figure 4.1, *Janthinobacterium* isolated on the cantilevers for 12 hours showed a high density of immobilized bacteria, but what looks like a biofilm. A gel-like substance also fills the room in between the legs of the triangular cantilevers. A possible explanation for the bent cantilevers could be that the biofilm causes the cantilevers to bend. During PDA treatment and incubation with bacteria, the chips containing the cantilevers is placed so that the chip is set on the surface, but the cantilevers points a little upward on each side. The cantilevers do not touch the surface during these preparations, and a high degree of biofilm production could possibly cause them to collapse and bend downwards.

The experiments performed on Day 1 and Day 2 of *Janthinobacterium* on both BSM and PGM (Figure 4.5a and c) were executed with cantilevers incubated with bacteria for ~24 hours. The figures show no clear differences between the these and the subsequent days, as deadhesion work is still low. All the same bacteria used for measurements in this thesis was collected from the same glycerol stocks and cultivated on the same type of TSA plates and in the same TSB media.

The reduced incubation time of *Janthinobacterium* from ~24 hours to 2 hours caused no more cantilevers to bend, and live/dead assays demonstrated a sufficiently high density of bacteria on the cantilevers (Figure 4.2a).

The density of immobilized *Janthinobacterium* and *Arthrobacter* on used probes was usually less dense than on unused probes, as represented for *Janthinobacterium* in Figure 4.2b and c and *Arthrobacter* in Figure 4.3b and c. Environmental stresses could be a possible explanation. As the bacteria-functionalized probes are moved towards and away from the mucin-coated surfaces, some of the bacteria may detach from the cantilever. In Figure 4.2c and 4.3c, the density of bacteria is observed to be higher on the cantilever legs than on the tips. A possible explanation for this distinction could be that bacteria detached from the cantilever when they contacted the mucins. All cantilevers shown in Figure 4.1, 4.2 and 4.3 are imaged from the side of the cantilever which made or would make contact with the mucin, and the lack of bacteria in Figure 4.2c and 4.3c could possibly be explained by the bacteria-mucin interaction, which has led to rupture of the interactions between the bacteria and the PDA layer and thus loss of the bacteria from the surface of the cantilever.

The detachment of bacteria from the surface of the cantilever during experiments would make the data interpretation complicated. For each measurement days, the same bacteria-immobilized probe is used during measurements of both mucins. If the bacteria fall off during experiments, it is possible that when inspecting the last mucin-coated surface, the density of bacteria on the probe is significantly reduced compared to the situation when inspecting the first surface. This is expected to result in less interaction observed for this surface compared to the first surface,

an observation that could be wrongly interpreted as a reduction in the interaction ability of the bacteria with the mucins immobilised onto the last surface inspected compared to the prior surfaces. Using the same probe when inspecting subsequent surfaces is in AFM experiments usually assumed to be an advantage, as this would minimize the variation due to differences in properties of the probe. However, as it appears that bacteria detach from the cantilever during experiment, the method needs to be optimized.

In Figure 4.3b representing *Arthrobacter*, there is a bright green fluorescent area at the tip of the cantilever, indicating a cluster of bacteria in this area of the probe. This cantilever was used in measurements on Day 2 on mucins treated with neuraminidase (Figure 4.4b and d). The deadhesion work measured with this tip is somewhat higher for both mucins, but it is exceptionally high for BSM (Figure 4.4b). The green area at the tip of this cantilever could explain the high deadhesion work measured this day.

5.2 Bacterial adhesion to BSM and PGM

The bacterial adhesion of *Arthrobacter* to BSM and PGM is presented in histograms showing the distribution of the observed magnitudes of deadhesion work (nN nm) (Figure 4.4 and 4.6). Both figures are based in the same histograms, but Figure 4.4 shows the separate measurement days for each mucin, while Figure 4.6 shows the collective interaction as well as common force-distance curves for each mucin.

Measurements of bacterial adhesion of *Arthrobacter* to BSM (Figure 4.4a) shows low deadhesion work for all 4 days. The days are also rather similar. Day 4 does however differ slightly from the other days, as the deadhesion work is more dispersed and there is no probability peak at the lower deadhesion work. Day 4 of bacterial interaction to PGM also differs from Day 1-3 (Figure 4.4c), but the deadhesion work is much higher. The same probe was used on the same day for both mucins, and the increased deadhesion work for both mucins could be caused by an increased bacterial density on the probe. A fifth day was also performed on *Arthrobacter* to PGM, but the deadhesion work differs even more on this day. A possible explanation for a greater distribution of the deadhesion work in both Day 4 and Day 5 could be an increased density of bacteria on the probe.

The bacterial adhesion of *Janthinobacterium* to BSM and PGM is presented in histograms showing the distribution of the observed magnitude of deadhesion work (nN nm) (Figure 4.5 and 4.7). Both figures represent the same histograms, but Figure 4.5 shows the separate measurement days for each mucin, and Figure 4.7 shows the total interaction of all days and common force-distance curves for each mucin.

Bacterial adhesion measurements of *Janthinobacterium* to both BSM (Figure 4.5a) and PGM (Figure 4.5c) shows low deadhesion work, most commonly under 30 nN nm. Day 3 and 4 of adhesion to BSM differs from the other days, as they do not have the same deadhesion work peak and are a little more distributed. As of Day 3, the incubation time of *Janthinobacterium* on the cantilever was reduced to 2 hours prior to measurements, and this could explain the change. Live/dead assays was however performed to analyse the bacterial density, which seemed to be sufficient. As the density could not be checked on the individual used probed prior to measurements, it could not be compared. It is possible that these probes had a higher density of bacteria, but the same interaction is not observed for Day 3 and Day 4 of *Janthinobacterium* to PGM (Figure 4.5c). If the increased interaction of Day 3 and 4 of BSM was caused by an increased bacterial density on the probe, this did not seem to affect attachment to PGM, and one could argue that *Janthinobacterium* has a higher deadhesion work to BSM than PGM.

The JPK glue used to attach the mica sheets on Day 1 and Day 2 of adhesion measurement of both *Janthinobacterium* and *Arthrobacter,* to both BSM and PGM, was empty after measurement Day2, and superglue was used as of Day 3. This glue was also used to attach all mica sheets treated with neuraminidase. As Day 3 and 4 differed from Day 1 and 2 for *Janthinobacterium* to BSM, a fifth day was completed to see if the same trend would continue, but it did not. Based on the result for both *Janthinobacterium* and *Arthrobacter*, the change of glue does not seem to affect the results obtained.

The force-distance curves for *Janthinobacterium* to BSM (Figure 4.7a) and PGM (Figure 4.7c) also shows little interactions and usually only a few single peaks. Based on the force-distance curves in Figure 4.6 a) and c), it seems like *Arthrobacter* established a greater interaction to both BSM and PGM in general compared to what is observed for *Janthinobacterium*. The histogram for *Arthrobacter* to BSM (Figure 4.4a) compared to *Janthinobacterium* to BSM (Figure 4.5a) shows a higher deadhesion work for *Arthrobacter*, and the same could be argued for PGM.

During this theses, the same mica sheets were used on the same measurement days for both *Arthrobacter* and *Janthinobacterium*, and the mucin density and distribution on the surface would also affect bacterial adhesion. The increased deadhesion work observed on Day 4 for *Arthrobacter* on BSM and PGM (Figure 4.4a and c) is also observed on Day 4 of *Janthinobacterium* on BSM (Figure 4.5a). The mucin properties could explain this change. The same pattern is however not followed for *Janthinobacterium* on PGM. During this thesis, the mucin density on the mica sheets was not controlled prior to measurements. They were all prepared the same way, and variation on mucin density on the surfaces is therefore not expected. However, insight into the mucin distribution and density prior to measurements would also be useful information when attempting to draw firm conclusions concerning the adhesive properties of the bacteria.

5.2.1 Bacterial adhesion to BSM and PGM treated with neuraminidase

Bacterial adhesion of *Arthrobacter* to BSM treated with neuraminidase is presented in Figure 4.4b and Figure 4.6b, and interaction to PGM treated with neuraminidase is presented in Figure 4.4d and Figure 4.6d.

When comparing adhesion to BSM, *Arthrobacter* seem to establish less interaction to the neuraminidase-treated mucin (Figure 4.4b). However, the deadhesion work measured for Day 2 and 3 is far greater than the other days. The same probes were used on Day 2 and 3 for PGM treated with neuraminidase (Figure 4.4d), and the measured deadhesion work is also greater here, even though the difference observed is not as pronounced. Day 2 for BSM is the one that stands out the most from the other measurements, and this is probably due to the bacterial density on the probe. Figure 4.3b represents the cantilever used during measurements on Day 2, and the concentration of green fluorescent on the tip could be the reason for the increased interaction. For PGM treated with neuraminidase (Figure 4.4d), it is mainly Day 3 that stands out. The increased deadhesion work is possibly caused by a dense assembly of bacteria which is expected to cause and increased adhesion to the mucins.

When comparing the force-distance curves for *Arthrobacter* on BSM and PGM in Figure 4.6, the curves obtained from measurements with the mucins (a and c) contains more multiple interactions than the curves from neuraminidase-treated mucins (b and d), which contains more single interaction. This also indicates that Arthrobacter interacts less with both BSM and PGM treated with neuraminidase. The exception is the largest curves placed furthest down in Figure

4.6 b and d. These were chosen from measurements with exceptionally high deadhesion work (Day 2 for BSM and Day 3 for PGM, Figure 4.4b) and d) respectfully)

Even though the deadhesion work seems to have somewhat decreased between *Arthrobacter* and BSM and PGM after neuraminidase treatment, bacterial interaction was still detected. If the bacteria originally form bonds with sialic acid units, this could mean that the neuraminidase treatment was not complete. As the bacteria still made interactions with the mucins, the removal of sialic acid was either not completely successful, or the bacteria could possibly bind to other components on the surface. Even so, it would be expected that the neuraminidase treatment would make the mucin-surface less charged, but this does not seem to have enhanced the bacterial adhesion. The overall bacterial interaction change is still not that big, and it is hard to determine the effect of the neuraminidase treatment.

When comparing bacterial adhesion of *Janthinobacterium* to BSM and PGM in Figure 4.5, the deadhesion work seems to be greater to both BSM and PGM treated with neuraminidase. When comparing BSM treated with neuraminidase (4.5b) and PGM treated with neuraminidase (4.5d), Day 4 and 5 of BSM both show a low deadhesion work, and the measured interactions is concentrated as high peaks. The same probe was used on Day 4 and 5 for PGM, and the same pattern can be seen here. Day 1 and 2 of BSM differs from the other days and shows a much wider distribution of deadhesion work. Day 1 and 2 is also more distributed for PGM, but not to the same extent. The force-distance curves of bacterial adhesion of *Janthinobacterium* to BSM and PGM treated with neuraminidase (Figure 4.7b and) also differ from BSM and PGM (Figure 4.7a and c). The force curves show more multiple interactions and higher rupture forces, and this is consistent with the deadhesion work presented in the histograms.

As there seem to be an overall increase in bacterial adhesion of *Janthinobacterium* to both BSM and PGM after treatment with neuraminidase, it appears as that the neuraminidase was able to affect the mucins to some extent. The details of the molecular interactions underlying the adhesive interactions of the bacteria are unknown, but the treatment seem to have enhanced the interaction. A possible explanation could be less electrostatic repulsions of the mucin coated layer due to the reduced density of charged units.

Comparing deadhesion work of *Janthinobacterium* to BSM treated with neuraminidase (Figure 4.5b), and *Arthrobacter* to BSM treated with neuraminidase (Figure 4.4b), reveal that Day 2 is exceptionally high for both. A high bacterial density on the cantilevers could be an explanation. The same mucin-coated mica sheet was used in these experiments, and this also applies for the other measurement days. This could explain the connection between the varying results. A greater density of mucins on the mica sheets could be an alternative explanation of the increased deadhesion work for BSM. However, during the experiments, the mucin concentration on the mica sheets was not investigated. The mica slides were all treated the same way, but they were not depicted or otherwise controlled. A method to analyse the concentration and distribution of mucins on the plates would have been useful to validate the sheets.

For both *Arthrobacter* and *Janthinobacterium,* there are distinct days that differ from the remaining days, and the probable cause is the bacterial density on the AFM probes. As per now, the immobilization of bacteria was not controlled prior measurements. Only a few probes were stained and visualised after measurements, and they were compared to unused probes. It would have been interesting to compare the bacterial density on the probes prepared for measurements, both prior to and after measurements, to see how well the PDA treatment worked, and how the AFM experiments affect the bacteria. A possible technique would be to use fluorescent proteins that stains the bacteria without affecting its adhesive properties, preferably proteins that enter the bacteria. The fluorescence could thus be studied before and after the experiment, providing information concerning the density and position of the bacteria both prior to and after the

experiments. It would also be interesting to image the mucin coated surfaces un a fluorescence microscope after completing the AFM experiments. The detection of fluorescence on the mucin coated surfaces after measurements, would indicate that fluorescently labelled bacteria had been transferred from the probe to the surface.

5.3 Single molecular pair interactions

The binding strength of single molecular pair interactions was also investigated in this thesis. The IDL version difordisjpkv31dr3 was used, and only single interactions in the force curves was selected. Many force curves were discarded, as single interactions could not be isolated. This resulted in a varying number of usable measurements. The number of single interactions also varies greatly between the different measurement days.

Scatter plots showing the loading rate (nN/s) relative to the rupture force (nN) of *Arthrobacter* is presented in Figure 4.8. The rupture forces determined are in all the scatter plots mainly located in an interval starting at 0,1 nN, and for BSM and BSM treated with neuraminidase, the interval goes up to ~0,4 nN, and for PGM and PGM treated with neuraminidase it goes up to ~0,3 nN. This same trend is also seen in histograms in Figure 4.9, where rupture force is presented in relation to probability. The histograms also show that the most probable rupture force lie just below 0,2 nN for all mucins (Figure 4.9). For BSM (Figure 4.9a), the highest peak lies at a rupture force of ~0,18 nN. There is also an additional peak at ~0,32 nN, which most likely represents rupture force of double interactions, as the rupture force is about twice as strong as the dominant peak. Based on Figure 4.8a, these measurements originate from Day 1, which deviates from the subsequent days. For BSM treated with neuraminidase (Figure 4.9b), there are multiple high peaks, but they are located at rupture forces ranging from ~0,14 – 0,2 nN. The dominant rupture forces of both PGM (Figure 4.9c) and PGM treated with neuraminidase (Figure 4.9d) range from ~0,15 to 0,17 nN.

The loading rates obtained when investigating the interaction between *Arthrobacter* and mucins (Figure 4.8) are primarily located in the 1-10 nN/s interval in all histograms, but Day 1 of BSM (Figure 4.8a) has a higher loading rate. Day 1 for PGM (Figure 4.8c) is only composed of one single measurement and cannot be used in comparison to BSM.

Based on all the scatter plots and the histograms presented in Figure 4.8 and 4,9, neuraminidase-treatment do not seem to have altered the single binding strength of *Arthrobacter*. This may indicate that the bacteria still interact with and binds to the same components, independently of the amount of sialic acid units and the precise mucin structure.

Scatter plots representing single molecular pair interactions of *Janthinobacterium* is presented in Figure 4.10. Fewer measurements were included for *Janthinobacterium* than *Arthrobacter*, as more curves were discarded due to the lack of single interactions. Even more curves were discarded for mucins treated with neuraminidase, as the probability for bacterial interactions and thus also the probability for multiple interactions, seemed to increase after neuraminidase treatment. As there were few single interactions, measurements of *Janthinobacterium* to all mucins, both BSM and PGM, and BSM and PGM treated with neuraminidase, is based on less than 280 measurements each, which makes it hard to determine any trends.

The rupture force distribution of *Janthinobacterium* is similar to that of *Arthrobacter*: There is a greater concentration of rupture force values at an interval starting at 0,1 nN, and for BSM and BSM treated with neuraminidase, the interval goes up to ~0,4 nN, and for PGM and PGM treated with neuraminidase it goes up to ~0,3 nN. However, the data is highly diverse. Day 4 and 5 of BSM (Figure 4.10a) is concentrated at a low rupture force, ~0,07- 0,15 nN. These

measurement also give rise to the peak in the rupture force distribution located at ~0,1 nN in the histogram representing BSM (Figure 4.11a). Day 1 (Figure 4.10a) has a more distributed rupture force at a higher value, and pulls the rupture force interval of BSM up to 0,4 nN. The measurements of Day 4 of PGM (Figure 4.10c) also have predominantly low rupture forces, but the number of force jumps analysed for this experimental series is low. Day 1 of PGM also differs from BSM as the rupture forces of the measurements are more distributed.

The single molecular pair interactions of *Janthinobacterium* to both BSM and PGM treated with neuraminidase (Figure 4.10b and d) is challenging to compare due to few measurements. The scatter plot of BSM treated with neuraminidase (Figure 4.10b) only includes a few measurements from Day 4 and 5. Day 5 seems to be concentrated at a rupture force <0,1 nN as well, but only 4 measurements were included for this day, thus making it unattainable to comparison. Most of the measurements of BSM treated with neuraminidase originates from Day 2, possessing a rupture force interval of ~0,1 – 0,4 nN, and the rupture force in the histogram representing BSM treated with neuraminidase (Figure 4.11b) is mainly based on this day.

The loading rate of *Janthinobacterium* in Figure 4.10 are primarily located in the 1-10 interval, as for Arthrobacter, but the loading rate of Day 1 of PGM (Figure 4.10c) reaching further above 10.

The rupture force of bacterial adhesion of *Janthinobacterium* is also represented in histograms showing the distribution of rupture forces (nN) (Figure 4.11). The low rupture force of Day 4 and Day 5 for BSM (Figure 4.10a) gives rise to the rupture force peak at ~0,1 nN (Figure 4.11a). This distinct peak is not observed for the other mucins. For BSM treated with neuraminidase, the highest peak lies at a rupture force of ~0,18 nN. For both PGM (Figure 4.11c) and PGM treated with neuraminidase (Figure 4.11d) the highest peak lies at ~0,17 nN. Disregarding BSM, the rupture force with the highest probability lie just below 0,2 nN, as for *Arthrobacter*. The rupture forces of BSM and BSM treated with neuraminidase (Figure 4.10 and 4.11) are the most diverse and show very different results. As previously discussed, the measurements of both days are scarce, and the result is based on too few measurement to determine any single molecular pair interactions. More single interactions of the bacterial adhesion need to be investigated to determine the rupture force of single interactions.

In previous studies, the binding strength of single molecular pair interactions of bacteria to glycans have been measured, and the rupture force has been determined to reside in the range of 20-180 pN, or 0,02-0,18 nN. Research of PGM to *Lactococcus lactis* also showed a rupture force of 180 ± 4, which agrees with the adhesive properties in this thesis (Formosa-Dague *et al.*, 2018).

6. Conclusion

The objective of this thesis was to investigate the adhesive properties of *Arthrobacter* and *Janthinobacterium* to mucins from bovine (BSM) and pig (PGM) before and after treatment with neuraminidase, by using AFM force microscopy. It was suspected that neuraminidase treatment would change and reduce the negative charge density of mucin, and thus the bacterial interaction. The removal of sialic acids would be expected to increase bacterial adhesion. It was desired that this information would provide information of the adhesive properties of the bacteria. The force curves obtained from AFM measurements was used to determine the total deadhesion work, and rupture force of single molecular pair interactions.

The binding strength of both *Arthrobacter* and *Janthinobacterium* to BSM and PGM was mostly weak. It did however seem as both bacteria had greater adhesive properties to BSM than PGM, but the observed differences are small. The bacterial adhesion of *Arthrobacter* to both BSM and PGM after neuraminidase treatment was reduced, and the force-distance curves contained fewer multiple interactions. It was expected that neuraminidase reduced the charge-density of the mucin, but it did not increase the adhesive properties. For *Janthinobacterium*, neuraminidase-treatment resulted in an increased bacterial adhesion to both mucins, and the force-distance curved contained more multiple interactions.

Some experimental steps were optimized during the experiment. The incubation time of *Janthinobacterium* on the cantilever was reduced to 2 hours due to experimental difficulties when isolated for 12-24 hours. The cantilever would bend and could not be used in experiments. The incubation time on TBS and TSA was also reduced to prevent formation of biofilms. The incubation time of *Arthrobacter* was maintained at ~ 24 hours. Live/dead assays were performed to observe bacterial viability and density. Whereas the viability was satisfactory, the bacterial density was lower on the used probes than the unused probes for both bacteria, which indicates that the bacteria detaches from the cantilever during experiments. The density should thus be optimized further in future experiments. The properties and density of mucins on the mica sheets should also be monitored before and after treatment with neuraminidase. All these steps would provide more secure results.

When measuring single molecular pair interactions, the rupture force of both bacteria had an interval of 0,1 – 0,3 or 0,4 nN. These results correlate with previous studies. However, as the data is based on few measurements, more experiments needs to be performed, and alternative methods which provides more single molecular pair interactions can be used. An alternative method to study single interactions could be to utilize single cell force spectroscopy, where a single cell is immobilised on the AFM probe (Beaussart *et al.*, 2014).

Bibliography

Ambort, D. *et al.* (2012) Calcium and pH-dependent packing and release of the gel-forming MUC2 mucin, *Proceedings of the National Academy of Sciences*, 109(15), pp. 5645-5650.

Bansil, R. and Turner, B. S. (2006) Mucin structure, aggregation, physiological functions and biomedical applications, *Current Opinion in Colloid & Interface Science*, 11(2), pp. 164-170.

Bansil, R. and Turner, B. S. (2018) The biology of mucus: Composition, synthesis and organization, *Advanced Drug Delivery Reviews*, 124, pp. 3-15.

Baos, S. C. *et al.* (2012) Distribution of sialic acids on mucins and gels: a defense mechanism, *Biophysical journal*, 102(1), pp. 176-184.

Barr, J. J. *et al.* (2015) Subdiffusive motion of bacteriophage in mucosal surfaces increases the frequency of bacterial encounters, *Proceedings of the National Academy of Sciences*.

Beaussart, A. *et al.* (2014) Quantifying the forces guiding microbial cell adhesion using single-cell force spectroscopy, *Nature Protocols*, 9(5), pp. 1049-1055.

Berg, J. *et al.* (2002) Lectins Are Specific Carbohydrate-Binding Proteins *Biochemistry. 5th edition.* New York: Freeman, WH.

Brockhausen, I. and Stanley, P. (2017) O-GalNAc Glycans, in Inglis, J. *e. a.* (ed.) *Essentials of Glycobiology, 3. edition.* New York: Cold Spring Harbor Laboratory Press, pp. 113-123.

Butt, H.-J. *et al.* (2005) Force measurements with the atomic force microscope: Technique, interpretation and applications, *Surface Science Reports*, 59(1), pp. 1-152.

Caldara, M. *et al.* (2012) Mucin Biopolymers Prevent Bacterial Aggregation by Retaining Cells in the Free-Swimming State, *Current Biology*, 22(24), pp. 2325-2330.

Chang, K.-C. *et al.* (2012) Atomic force microscopy in biology and biomedicine, *Tzu Chi Medical Journal*, 24(4), pp. 162-169.

Corfield, A. P. (2015) Mucins: A biologically relevant glycan barrier in mucosal protection, *Biochimica et Biophysica Acta (BBA) - General Subjects*, 1850(1), pp. 236-252.

Dey, S. and Paul, P. A. (2018) Influence of metal ions on biofilm formation by Arthrobacter sp. SUK 1205 and evaluation of their Cr(VI) removal efficacy, *International Biodeterioration & Biodegradation*.

Ding, Y. H. *et al.* (2016) Mussel-inspired polydopamine for bio-surface functionalization, *Biosurface and Biotribology*, 2(4), pp. 121-136.

Dufrêne, Y. F. and Hinterdorfer, P. (2008) Recent progress in AFM molecular recognition studies, *Pflügers Archiv - European Journal of Physiology*, 456(1), pp. 237-245.

Dufrêne, Y. F. (2017) Microbial Nanoscopy: Breakthroughs, Challenges, and Opportunities, *ACS Nano*, 11(1), pp. 19-22.

Dunne, W. M., Jr. (2002) Bacterial adhesion: seen any good biofilms lately?, *Clinical microbiology reviews*, 15(2), pp. 155-166.

Eaton, P. and West, P. (2010) *Aromic Force Microscopy*. New York: Oxford University Press.

Erdal, M. S. (2019) *Bacterial adhesion to mucosal surfaces*. Thesis, Norges teknisk-naturvitenskapelige universitet.

Eschbach, M. *et al.* (2003) Members of the genus Arthrobacter grow anaerobically using nitrate ammonification and fermentative processes: anaerobic adaptation of aerobic bacteria abundant in soil, *FEMS Microbiology Letters*, 223(2), pp. 227-230.

Esteban, M. (2012) An Overview of the Immunological Defenses in Fish Skin, *ISRN Immunology*, 2012.

Formosa-Dague, C. *et al.* (2018) The Role of Glycans in Bacterial Adhesion to Mucosal Surfaces: How Can Single-Molecule Techniques Advance Our Understanding?, *Microorganisms*, 6(2), pp. 39.

Fu, H. *et al.* (2014) Research Progress on the Actinomyces arthrobacter, *Advances in Microbiology*, 04, pp. 747-753.

Gillis, M. and Logan, N. A. (2015) Janthinobacterium *Bergey's Manual of Systematics of Archaea and Bacteria.* pp. 1-12.

Glanz, V. Y. *et al.* (2018) Inhibition of sialidase activity as a therapeutic approach, *Drug design, development and therapy*, 12, pp. 3431-3437.

Hinterdorfer, P. and Dufrêne, Y. F. (2006) Detection and localization of single molecular recognition events using atomic force microscopy, *Nature Methods*, 3(5), pp. 347-355.

Haack, F. S. *et al.* (2016) Molecular Keys to the Janthinobacterium and Duganella spp. Interaction with the Plant Pathogen Fusarium graminearum, *Frontiers in Microbiology*, 7(1668).

Kasas, S. and Dietler, G. (2017) Chapter Six - Analysis of Data Gleaned by Atomic-Force Microscopy, in Ikai, A. (ed.) *The World of Nano-Biomechanics (Second Edition).* Amsterdam: Elsevier, pp. 95-109.

Lichtman, J. W. and Conchello, J.-A. (2005) Fluorescence microscopy, *Nature Methods*, 2(12), pp. 910-919.

Lindén, S. *et al.* (2008) Mucins in the mucosal barrier to infection, *Mucosal immunology*, 1, pp. 183-197.

Liu, Y. *et al.* (2014) Polydopamine and Its Derivative Materials: Synthesis and Promising Applications in Energy, Environmental, and Biomedical Fields, *Chemical Reviews*, 114(9), pp. 5057-5115.

Madsen, J. B. *et al.* (2016) Structural and Mechanical Properties of Thin Films of Bovine Submaxillary Mucin versus Porcine Gastric Mucin on a Hydrophobic Surface in Aqueous Solutions, *Langmuir*, 32(38), pp. 9687-9696.

Majtner, T. (2015) *Texture-Based Image Description in Fluorescence Microscopy*.

Oh, W. T. *et al.* (2019) Janthinobacterium lividum as An Emerging Pathogenic Bacterium Affecting Rainbow Trout (Oncorhynchus mykiss) Fisheries in Korea, *Pathogens (Basel, Switzerland)*, 8(3), pp. 146.

Pantanella, F. *et al.* (2007) Violacein and biofilm production in Janthinobacterium lividum, *Journal of Applied Microbiology*, 102(4), pp. 992-999.

Pape, P. G. (2011) 29 - Adhesion Promoters: Silane Coupling Agents, in Kutz, M. (ed.) *Applied Plastics Engineering Handbook.* Oxford: William Andrew Publishing, pp. 503-517.

Ribet, D. and Cossart, P. (2015) How bacterial pathogens colonize their hosts and invade deeper tissues, *Microbes and Infection*, 17(3), pp. 173-183.

Sanderson, M. J. *et al.* (2014) Fluorescence microscopy, *Cold Spring Harbor protocols*, 2014(10).

Sicard, J.-F. *et al.* (2017) Interactions of Intestinal Bacteria with Components of the Intestinal Mucus, *Frontiers in cellular and infection microbiology*, 7, pp. 387-387.

Sigma-Aldrich (2020a) Mucin from bovine submaxillary glands. Downloaded May 19 2020 from https://www.sigmaaldrich.com/catalog/product/sigma/m3895?lang=en&region=NO

Sigma-Aldrich (2020b) Mucin from porcine stomach. Downloaded May 19 2020 from https://www.sigmaaldrich.com/catalog/product/sigma/m1778?lang=en&region=NO&cm_sp=Insite-_-caContent_prodMerch_gruModel-_-prodMerch10-1.

Sigma-Aldrich (2020c) α(2→3,6,8,9) Neuraminidase from Arthrobacter ureafaciens. Downloaded June 10 2020 from https://www.sigmaaldrich.com/catalog/product/sigma/n3786?lang=en&region=NO.

Stencel-Baerenwald, J. E. *et al.* (2014) The sweet spot: defining virus-sialic acid interactions, *Nature reviews. Microbiology*, 12(11), pp. 739-749.

Stones, D. H. and Krachler, A. M. (2016) Against the tide: the role of bacterial adhesion in host colonization, *Biochemical Society transactions*, 44(6), pp. 1571-1580.

Tyo, A. *et al.* (2019) Development and Characterization of an Antimicrobial Polydopamine Coating for Conservation of Humpback Whales, *Frontiers in Chemistry*, 7(618).

Van den Abbeele, P. *et al.* (2012) Incorporating a mucosal environment in a dynamic gut model results in a more representative colonization by lactobacilli, *Microbial biotechnology*, 5(1), pp. 106-115.

Wang, B. *et al.* (2017) The Human Microbiota in Health and Disease, *Engineering*, 3(1), pp. 71-82.

Zhang, C. *et al.* (2017) Deposition and Adhesion of Polydopamine on the Surfaces of Varying Wettability, *ACS Applied Materials & Interfaces*, 9(36), pp. 30943-30950.

Zhang, J. X. J. and Hoshino, K. (2019) Chapter 5 - Optical transducers: Optical molecular sensing and spectroscopy, in Zhang, J. X. J. and Hoshino, K. (ed.) *Molecular Sensors and Nanodevices (Second Edition).* Academic Press, pp. 231-309.

Ølnes, Å. S. (2019) *Use of nanobiotechnology tools to study the mechanisms underlying bacterial adhesion to mucins*. Thesis, Norges teknisk-naturvitenskapelige universitet.

Appendix

Solutions and media

Recipes of medias and buffers used in this thesis is listed in the tables below.

Table A1: Composition of tryptic soy agar (TSA)

Components	**Amount**
Tryptic soy broth	22.5 g
Agar	11.25 g
dH2O	750 mL

Table A2: Composition of salmon growth media (SGM)

Components	**Amount (mL)**
$MgSO_4$	10
KCl	10
$NaHCO_3$	10
$CaSO_4$	200
dH_2O	770

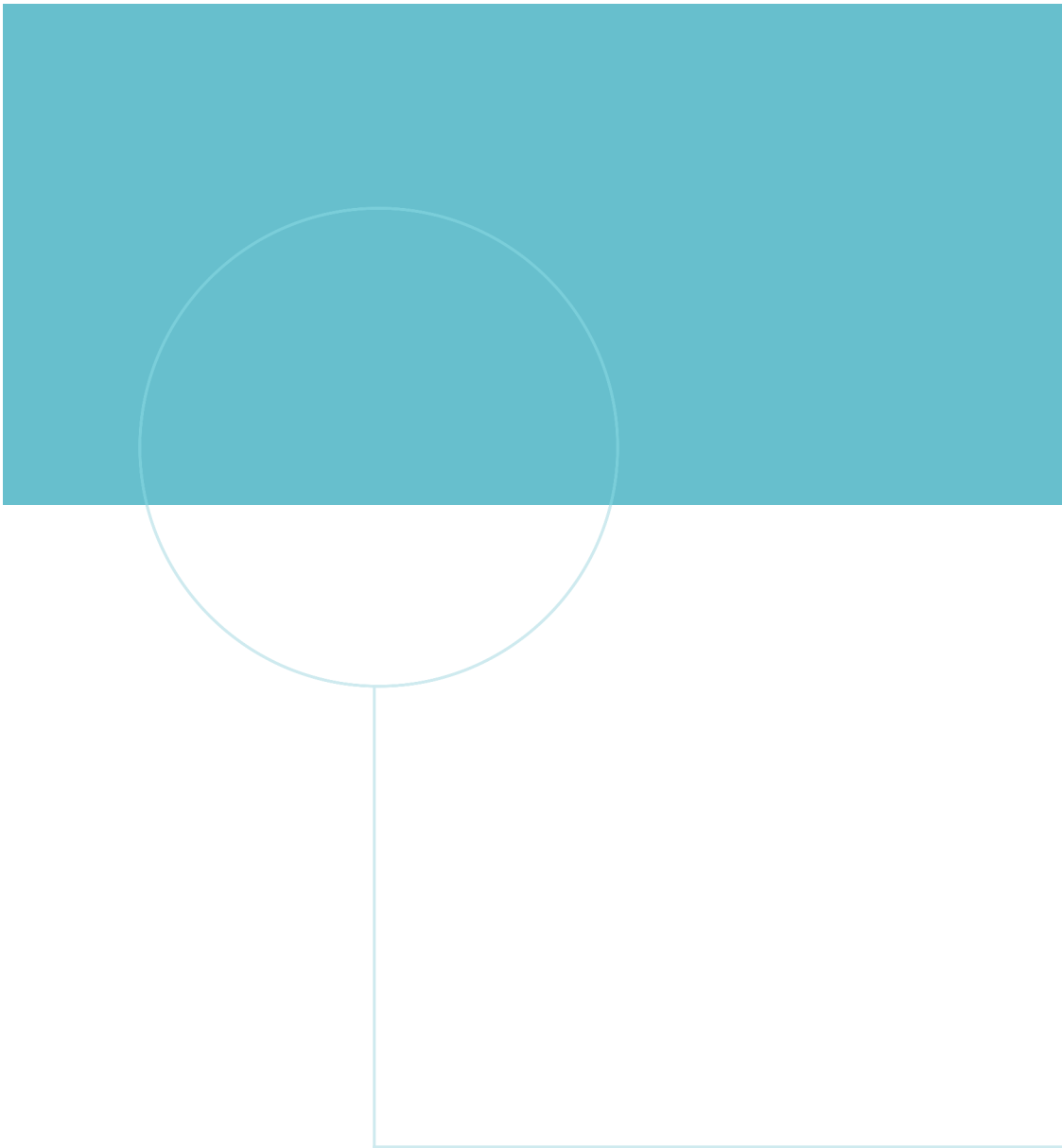

NTNU

Norwegian University of
Science and Technology